

Supporting Information (SI)

Highly Selective Detection of Hypochlorous Acid by a Bis-Heteroleptic Ru(II) Complex of Pyridyl-1,2,3-Triazole Ligand via C(sp²)-H Hydroxylation

Bhaskar Sen,[†] Sanjoy Kumar Sheet,[†] Sumit Kumar Patra,[†] Debaprasad Koner,[§] Nirmalendu Saha,[§] Snehadrinarayan Khatua^{†}*

[†]Centre for Advanced Studies, Department of Chemistry, [§]Department of Zoology, North Eastern Hill University, Shillong, Meghalaya-793022, India.

Email: snehadri@gmail.com; skhatua@nehu.ac.in

Table of Contents

Contents	Page no
1. General Methods and Experiments	S2-S5
2. Synthetic Procedures	S6
3. NMR, ESI mass, UV-vis, PL Spectra and Crystal structure	
a) NMR spectra of azide/ tetrazole (A/B)	S7
b) NMR and ESI mass- spectra of BtPT ligand	S8-S9
c) NMR and ESI mass spectra of Ru-1	S9-S12
d) Normalized absorbance and PL spectra of Ru-1 and Ru-1-OH	S12
e) UV-vis selectivity of Ru-1 with ROS, RNS, anions	S13
f) UV-vis titration of Ru-1 with HOCl	S14
g) Calculation of detection limit	S14-S15
h) Competitive study of ROS/RNS/anions in PL spectroscopy	S15
i) Emission Lifetime measurement of Ru-1 and Ru-1-OH	S16
j) pH effect on Ru-1 and Ru-1-OH	S16
k) Time course for Ru-1 in presence of HOCl and PL titration in DMSO	S17
l) ESI mass spectrum of Ru-1 and NaOCl reaction mixture	S17
m) NMR and ESI mass spectra of Ru-1-OH	S18-S19
n) UV-vis and PL spectra of Ru-2 in presence of HOCl	S20
o) ESI mass spectrum of Ru-2 and NaOCl reaction mixture	S21
p) PL titration of BtPT with HOCl	S21
q) ¹ H NMR titration of BtPT ligand with NaOCl	S22
r) Normalized absorbance and PL spectra of Ru-3	S22
s) NMR and ESI mass spectra of Ru-3	S23-S24
t) Crystal structure of Ru-3·H₂O	S24
4. List of selected probes for HClO/ClO⁻ detection	S25-S27
5. X-ray crystallography	S27-S30
6. Computational study	S31-S41
7. Cell viability study	S41
8. References	S42

1. General Methods and Experiments

Preparation of ROS and RNS solutions

Generation of HOCl/OCl⁻: The source of HOCl was commercial bleach. The concentration of the HOCl stock solution was determined by measuring the absorbance at 235 nm with a molar extinction coefficient of 100 M⁻¹ cm⁻¹ in PBS buffer (pH-7.4).

Generation of H₂O₂: The concentration of stock H₂O₂ solution was obtained from the absorbance at 240 nm with a molar extinction coefficient of 43.6 M⁻¹ cm⁻¹.

Generation of ^tBuOOH: The commercial available tert-Butyl hydroperoxide solution was diluted with double distilled water and used as a source of ^tBuOOH.

Generation of O₂^{•-}: Superoxide radical anion was generated from solid potassium superoxide (KO₂).

Generation of [•]OH: Fenton reaction is used for the generation of hydroxyl radical ([•]OH). An aqueous solution of ferrous sulphate was added to 10 times higher concentrated H₂O₂ solution and the concentration of [•]OH was determined as same equivalent to the Fe(II) concentration.

Generation of peroxynitrite (ONOO⁻): A mixture of sodium nitrite (0.6 M) and hydrogen peroxide (0.7 M) solution was acidified with hydrochloric acid (0.6 M) and followed by the immediate addition of sodium hydroxide (1.5 M) solution. The resulting solution was kept at lower than -18 °C. The solution was liquefied instantly before use. The concentration of the stock solution was measured in 0.1 M NaOH by determining the absorbance at 302 nm with a molar extinction coefficient of 1670 M⁻¹cm⁻¹.

Generation of NO[•]: SNP (Sodium nitroferricyanide (III) dihydrate) was used for generation of nitric oxide.

Generation of singlet oxygen (¹O₂): ¹O₂ was generated by mixing of 1 mM NaClO with 1 mM H₂O₂.

Calculation of Detection Limit

The detection limit was calculated based on titration data. To determine the S/N ratio, the standard deviation of blank solution was calculated with 10 replicate data of **Ru-1** without

addition of HOCl in PL spectroscopy. Finally, the detection limit (DL) of **Ru-1** for HOCl was determined from the following equation.

$$DL = 3\sigma/K$$

Where σ is the standard deviation of the blank solution and K is the slope obtained from the plot of calibration curve.

Calculation of Quantum Yield

The quantum yield of **Ru-1** and **Ru-1-OH** were determined in PBS buffer (pH 7.4, 10 mM, containing 5% DMSO) and [Ru(bpy)₃](PF₆)₂ was used as a reference (Φ_R of 0.062 in CH₃CN).^[1] The quantum yield is calculated according to the following equation:

$$\Phi_S = \Phi_R \times \frac{1 - 10^{-A_R}}{1 - 10^{-A_S}} \times \frac{I_S}{I_R} \times \frac{\eta_S^2}{\eta_R^2}$$

Where, Φ_S and Φ_R are respective the quantum yields of the sample and reference. I_S and I_R are represented the area under emission spectra of the sample and the reference respectively. A_S and A_R are the absorbance of the sample and the reference at the excitation wavelength, respectively. η_S and η_R are the refractive index of the solvents used for the sample and reference, respectively.

Calculation of excited states lifetimes

The luminescence lifetime of **Ru-1** before and after addition of HOCl was measured using a time-correlated single photon counting (TCSPC) spectrometer from Lifespec II instrument (Edinburgh Ltd., U.K.). The samples are excited at 470 nm using a picoseconds laser diode. The fluorescence decays were monitored at the corresponding emission maxima as observed in the steady state fluorescence measurement. The data were analysed using FAST decay analysis software from Edinburgh Instruments. All the fluorescence decays were fitted with a biexponential function considering a χ^2 value close to 1, which is an indication of good fitting. Experimental time-resolved luminescence data were calculated using the following multiexponential decay equation

$$\langle \tau \rangle = \sum a_i \tau_i$$

Whereas, a_i is the amplitude of the i^{th} decay component ($a_i = \alpha_i / \sum \alpha_i$) and τ_i is the excited state luminescence life time of the i^{th} component.

Electrochemical studies

For electrochemical analysis, we have taken the three electrodes cell system, containing a Pt working electrode, a Pt wire auxiliary electrode and an Ag wire as a pseudo-reference electrode. Experiments were carried out on a 1.0 mM of **Ru-1** and **Ru-1-OH** solutions in a dry and degassed acetonitrile with 0.1 M tetra-n-butylammonium perchlorate (Bu_4NClO_4) as the supporting electrolyte. To compare the oxidation potential shift between **Ru-1** and **Ru-1-OH**, the cyclic voltammetry data of $[\text{Ru}(\text{phen})_3](\text{PF}_6)_2$ was also collected under the same experimental conditions. After each experiment, the electrochemical potential window was calibrated using ferrocene as the internal standard. The redox potential of the ferrocene/ferrocenium (Fc/Fc^+) couple was taken as +0.400 V vs Ag wire electrode.^[2] All the reported potentials were measured at a scan rate of 100 mV s^{-1} .

Computational Studies

The geometry optimization of **Ru-1** and **Ru-1-O⁻** (deprotonated form in solution) were performed with the Gaussian 09 program package, using density functional theory (DFT). The B3LYP/6-31G (d,p)^[3] basis set was used for C, H, N, O, S together with the LANL2DZ^[4] for ruthenium. The geometry was fully optimized in the ground states. Time dependent density functional theory (TD-DFT) calculations using the polarizable continuum model (PCM)^[5] non equilibrium version were performed with a spin-restricted formalism to examine low-energy excitations at the ground-state geometry in water at the same level of calculation, as employed for geometry optimizations. The triplet states TDDFT calculations using the optimized triplet state geometry at the same level [B3LYP/6-31G (d,p)] associated with the PCM (H_2O) were employed for singlet–triplet transitions to study the nature of the non-emissive and emissive states of **Ru-1** and **Ru-1-O⁻**, respectively.

Cytotoxicity Study

The Cytotoxicity test of the **Ru-1** against HEK-293T cells was determined by MTT assay as described by Mosmann, (1983) in a 96-well cell culture plate. The cells were seeded in a 96-well plate containing 2 ml of DMEM (Dulbecco's Modified Eagle Medium) at a density of 4×10^3 cells/well and incubated at 37 °C, 5% CO_2 incubator. Cells were treated with different concentration of **Ru-1** (0, 10, 25, 50, and 100 μM) at 70% confluency and incubated for 24 h. After incubation in media, the old media was replaced by same volume of serum free DMEM media and MTT salt was added in medium to a final concentration of 0.5 mg/ml. The plate was incubated for 4 hours at 37 °C until intracellular purple formazan crystals were visible

under microscope. After incubation, the media was discarded and 200 µl of DMSO was added in well. The absorbance change was monitored at 570 nm using iMark™ (Bio-Rad, USA) microplate absorbance reader. Readings were taken in triplicate and the % cell viability was calculated for samples and controls based on the following formula:

$$\% \text{ cell viability} = (R_{\text{sample}} - R_0)/(R_{\text{ctrl}} - R_0) \times 100$$

Where, R_{sample} is the absorbance in the presence of **Ru-1**. R_{ctrl} is the absorbance of in the absence of the sample (vehicle control). R_0 is the averaged background (noncell control) absorbance.

Cell culture and Exogenous and Endogenous HOCl Imaging

Cells were seeded at normal confluency (~10%) in 12 well sterile culture plates on poly-L-lysine coated coverslips containing 2 ml of DMEM (Dulbecco's Modified Eagle Medium) medium and incubated inside a CO₂ incubator at 37 °C with 5% CO₂ supplemented with 1% streptomycin penicillin and 10% FBS (Fetal Bovine Serum). When the cells were approximately 70% confluent, the media was replaced with fresh media.

For the control experiment, the cells were only treated with **Ru-1** (50 µM) for 15 min. For the imaging of the exogenous HOCl, the HEK293T cells were incubated with **Ru-1** (50 µM, 15 min) and then treated with aqueous NaOCl (50 µM, 15 min). For the detection of endogenously produced HOCl, the HEK293T cells were treated with lipopolysaccharide (LPS, 1 µg/ml)^[6] and kept under incubation for 2 h. Then, the cells were treated with **Ru-1** (25 µM, 15 min). Similarly, to determine the paraquat-stimulated endogenously generated HOCl, the cells were treated with paraquat (1 mM) for 1.5 h and subsequent addition of **Ru-1** (25 µM) for another 15 min. After the all treatment finally the cells were washed two times with 500 µl of HBSS (Hank's Balanced Salt Solution) and fixed with chilled absolute ethanol. The fixed cells were washed further three times with 500 µl of HBSS to remove residual ethanol. Finally, the cell containing coverslips were mounted on glass slides. Imaging studies of these three experiments were performed by conducting fixed-cells imaging on confocal laser scanning microscopy (Leica, TCS SP5, Germany). Nucleus staining dye DAPI was used in all experiments. Images were taken using 405 nm (for DAPI) and 488 nm (**Ru-1**) excitation and emission windows of 420–510 nm (blue) and 510–630 nm (red). Cross-talk of fluorochromes was excluded by the use of the acous to optical tunable filter.

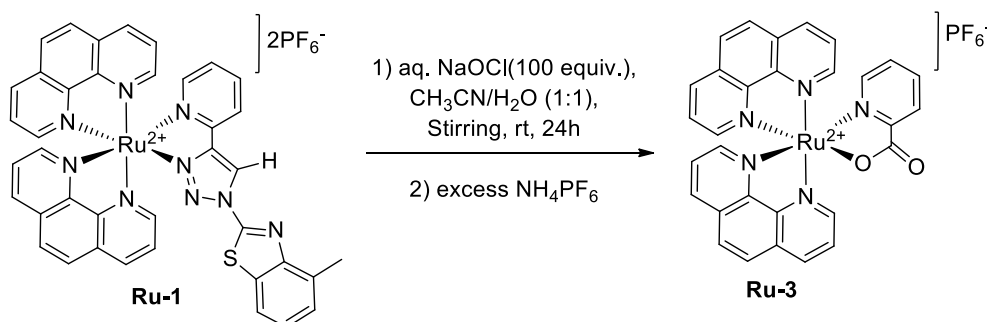
2. Synthetic Procedures

Synthesis of [Bis(1,10-phenanthroline)(2-(1-methyl-1H-1,2,3-triazol-4-yl)pyridine)]ruthenium(II) dihexafluorophosphate, **Ru-2**.

The control probe **Ru-2** was synthesized following the reported literature procedure.^[7]

Synthesis of [Bis(1,10-phenanthroline)(2-pyridinecarboxylate)]ruthenium(II) dihexafluorophosphate, **Ru-3**

The complex **Ru-1** (0.07 mmol, 0.073g) was dissolved in 1:1 acetonitrile/water mixture (10 ml). To this stirred solution, an aqueous NaOCl (7 mmol, 30 ml) was added dropwise. After 24 h stirring, the organic solvent was evaporated and treated with an excess NH_4PF_6 . The crude precipitate was then purified by silica gel column chromatography (0.2% saturated KNO_3 : 9.8% H_2O : 90% CH_3CN as an eluent) to afford dark red coloured **Ru-3** in a good



Scheme S1. Synthetic approach to **Ru-3** complex

yield (0.031g, 60%) (Scheme S1). The diffraction-quality single crystals of complex **Ru-3** were obtained from an acetone and water (2:1) mixture after five days. Anal. Calcd. for $\text{C}_{30}\text{H}_{22}\text{F}_6\text{N}_5\text{O}_3\text{PRu}$ ($M_w = 746.56$): C, 48.26; H, 2.97; N, 9.38. Found: C, 48.17; H, 2.92; N, 9.26. FTIR in KBr disc (ν/cm^{-1}): 3435, 1641(C=O stretching), 1122, 841 (PF_6 stretching), 603. ESI-MS: m/z calculated for $[\text{C}_{30}\text{H}_{20}\text{N}_5\text{O}_2\text{Ru}]^+$ 584.07; found: 584.07. ^1H NMR (400 MHz, CD_3CN): δ (ppm) = 9.24 (d, $J = 6.4$, 1H), 8.64 (t, $J = 8.0$ Hz, 2H), 8.38 (m, 3H), 8.23 (m, 2H), 8.16 (m, 2H), 8.04 (m, 3H), 7.85 (m, 3H), 7.48 (d, $J = 5.4$ Hz, 1H), 7.44 (d, $J = 8.0$ Hz, 1H), 7.42 (d, $J = 8.0$, 1H), 7.23 (t, $J = 7.3$ Hz, 1H). ^{13}C NMR (100 MHz, CD_3CN): δ (ppm) = 173.1, 155.3, 155.1, 153.8, 153.2, 152.7, 152.0, 150.7, 149.7, 149.3, 138.1, 136.6 (2C), 136.2, 135.4, 131.8, 131.6, 131.5, 131.3, 129.0, 128.8 (2C), 128.7, 128.6, 127.7, 128.6, 127.8, 126.7, 126.2, 125.8.

3. NMR, ESI mass, UV-vis, PL Spectra and Crystal structure

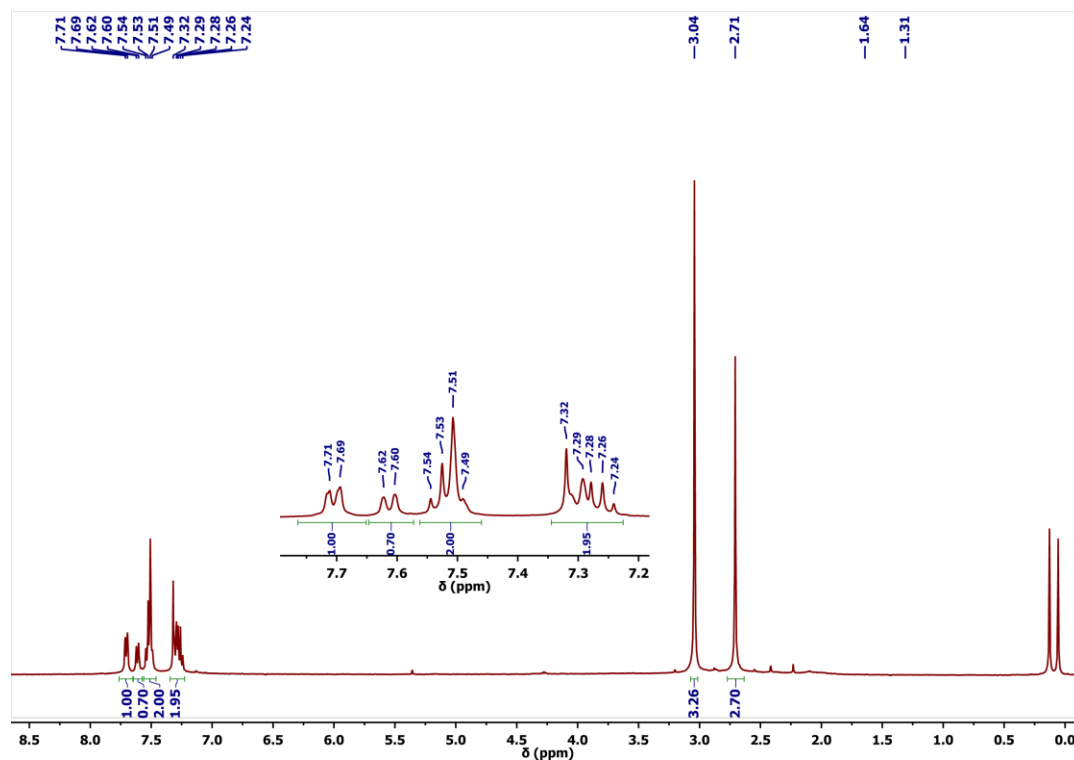


Figure S1. ¹H NMR spectrum of A/B in CDCl₃ (400 MHz).

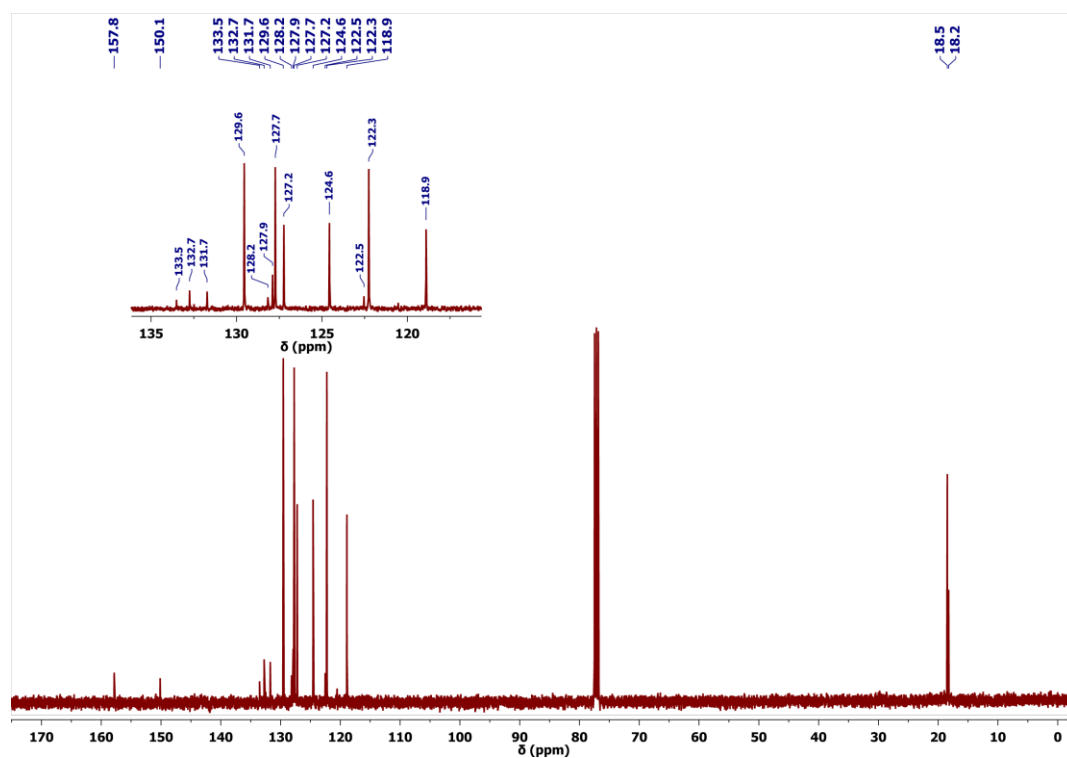


Figure S2. ¹³C NMR spectrum of A/B in CDCl₃ (100 MHz).

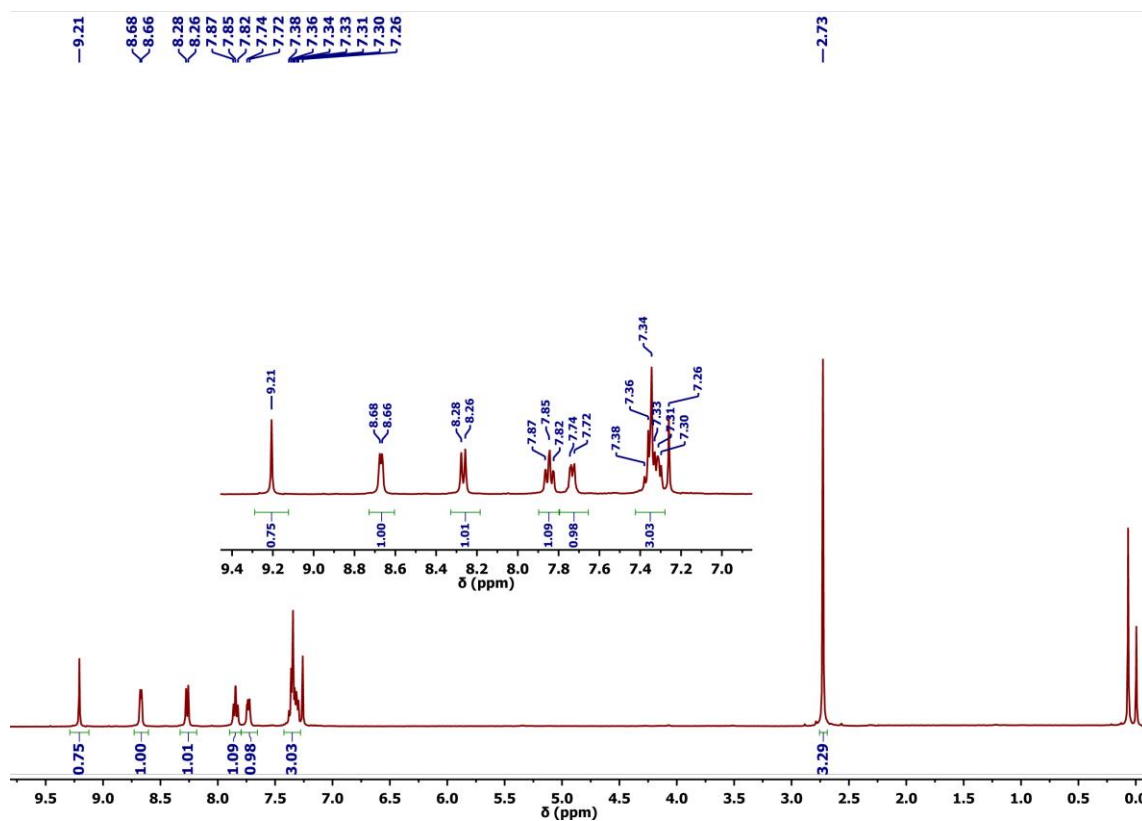


Figure S3. ¹H NMR spectrum of **BtPT** in CDCl₃ (400 MHz).

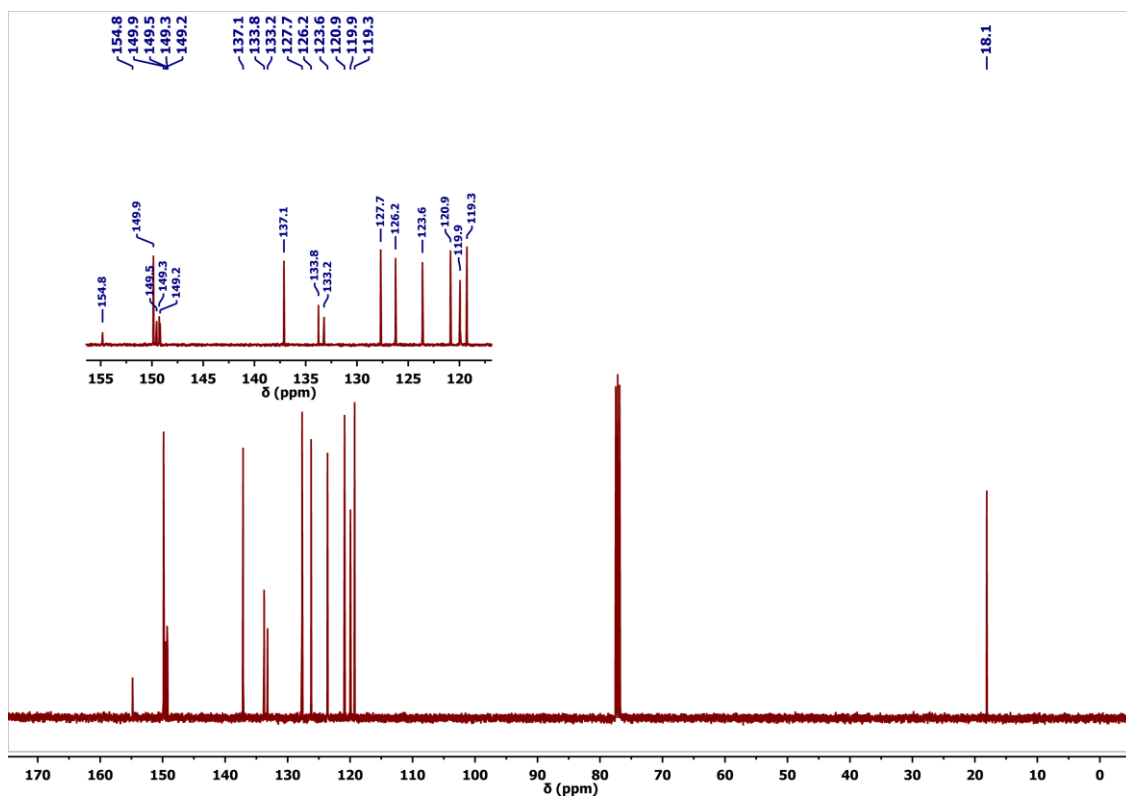


Figure S4. ¹³C NMR spectrum of **BtPT** in CDCl₃ (100 MHz).

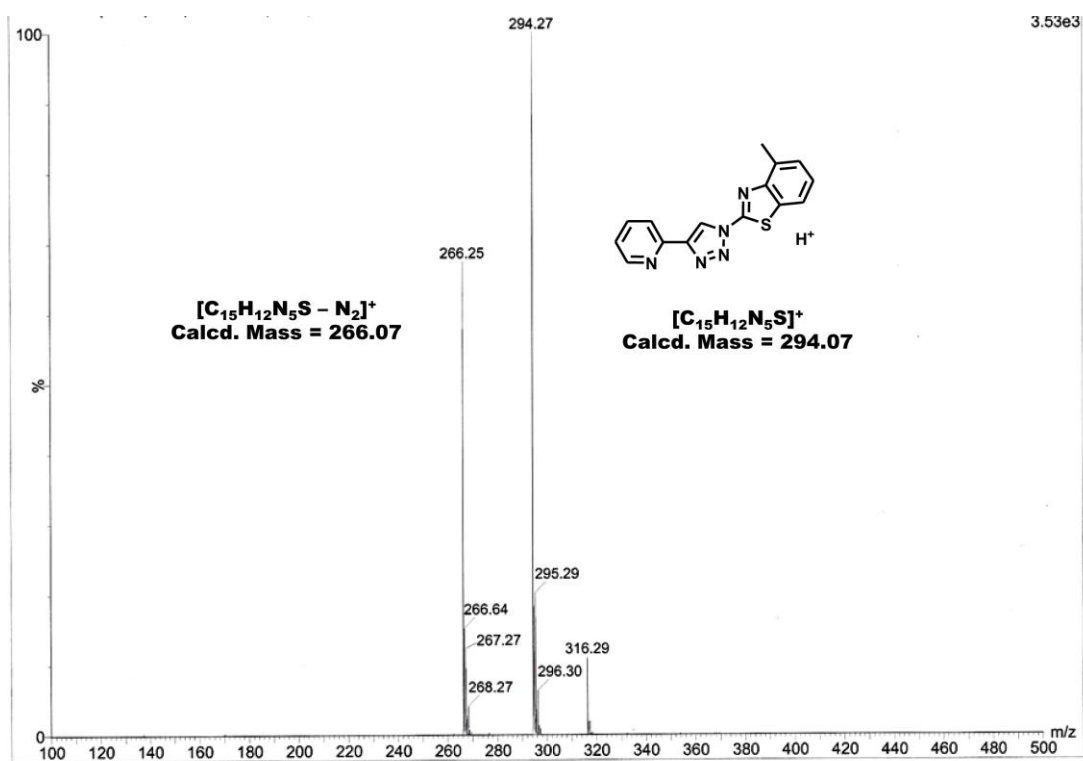


Figure S5. ESI mass spectrum of BtPT in CHCl_3 .

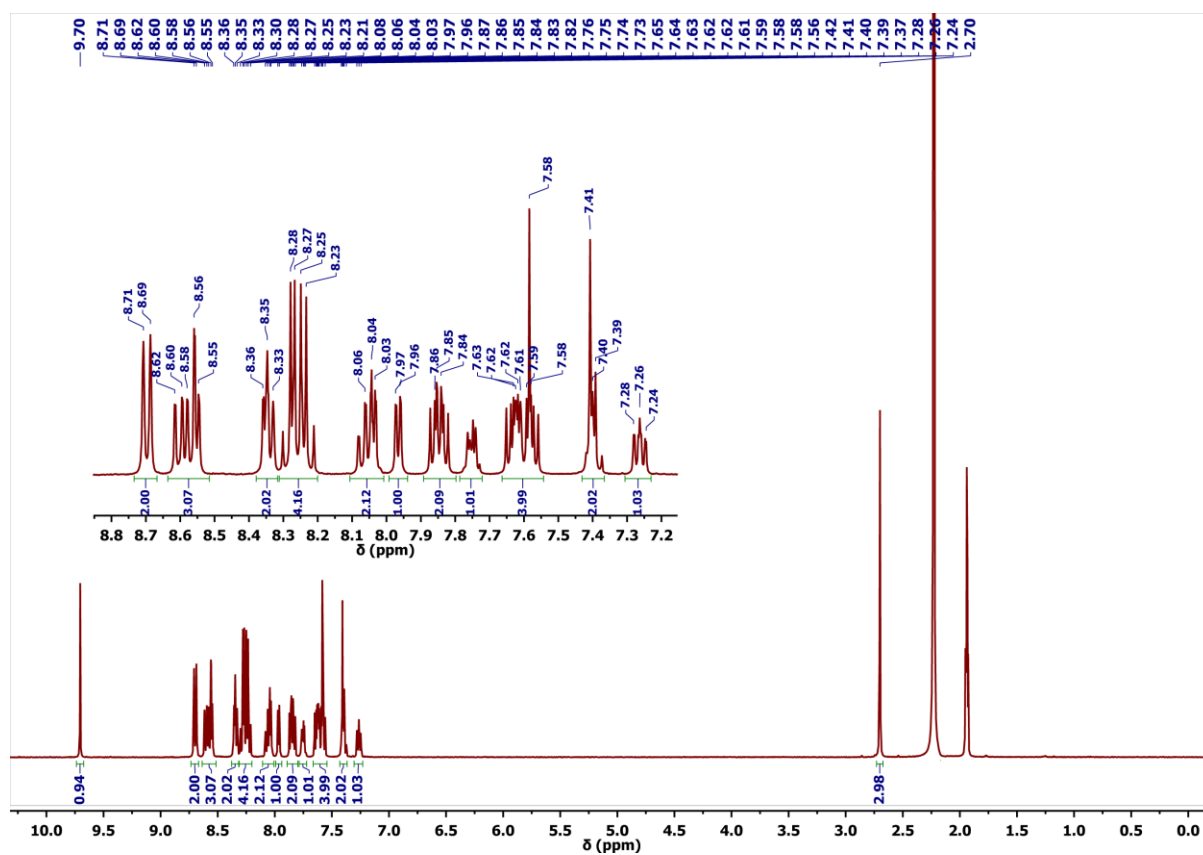


Figure S6. ^1H NMR spectrum of Ru-1 in CD_3CN (400 MHz).

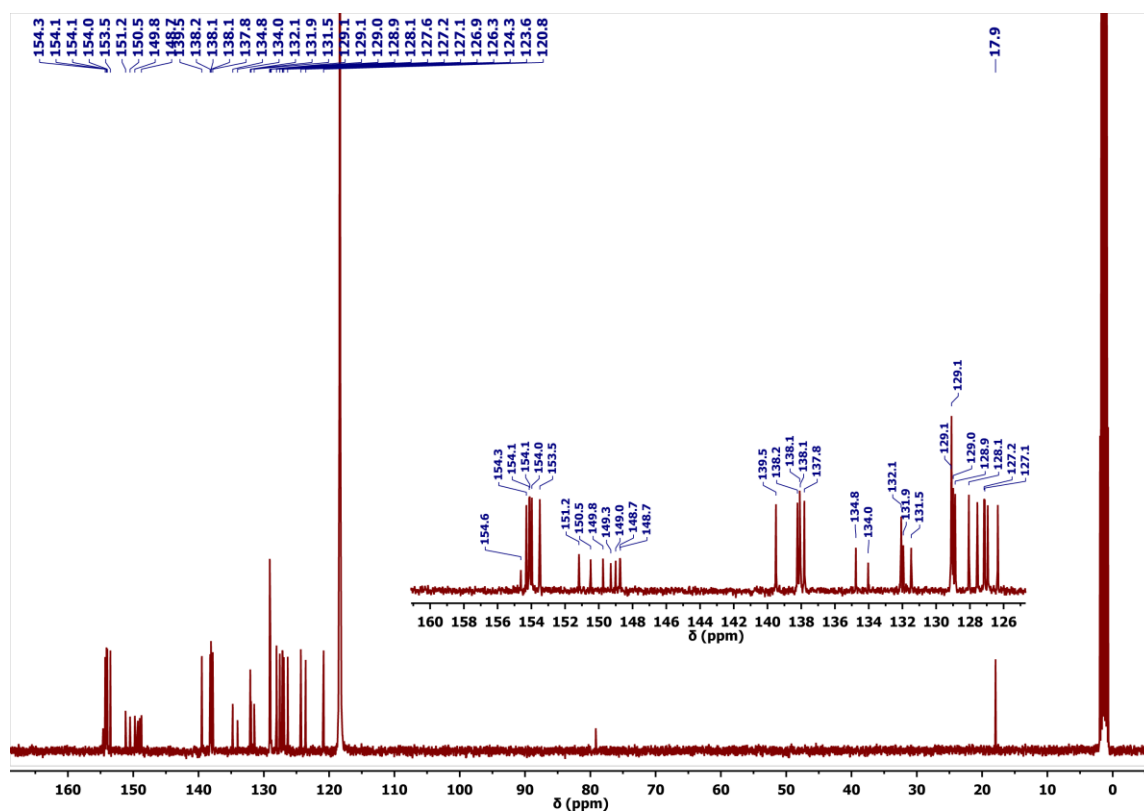


Figure S7. ^{13}C NMR spectrum of **Ru-1** in CD_3CN (100 MHz).

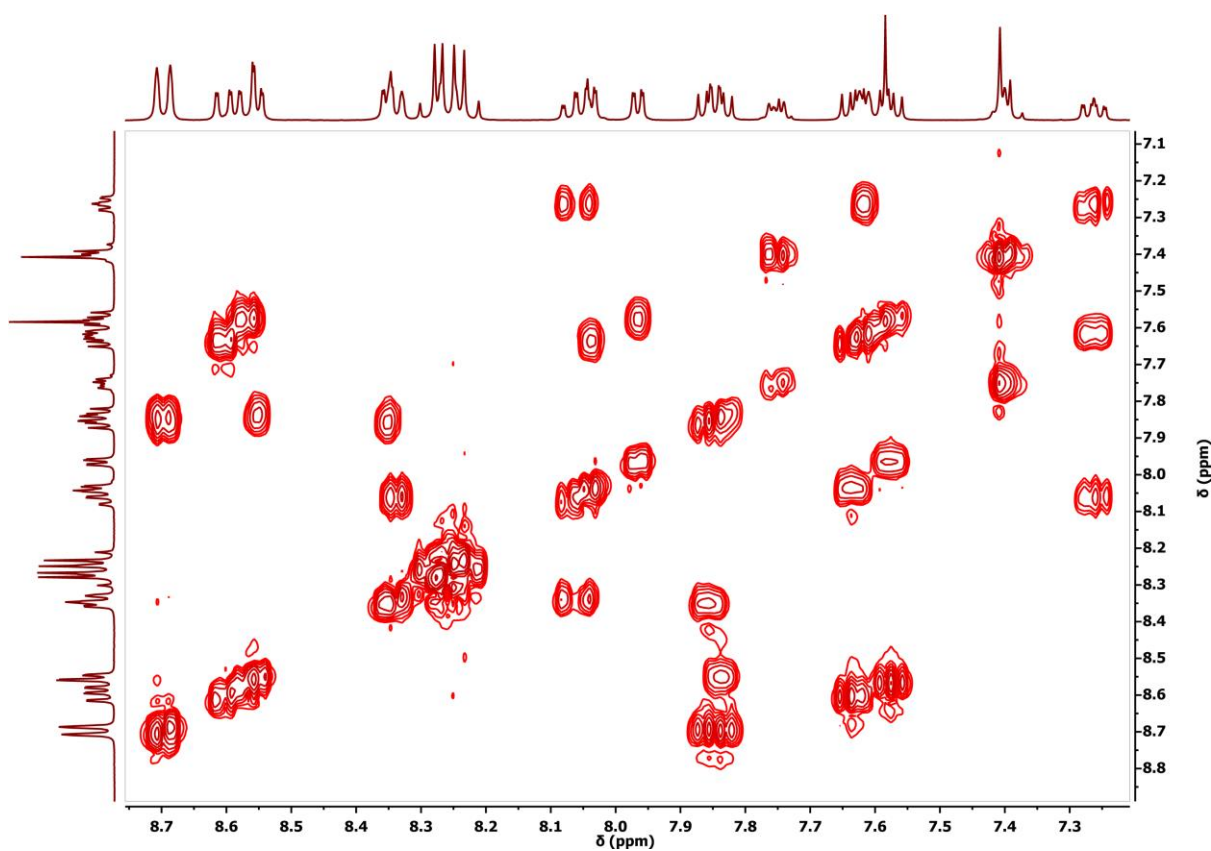


Figure S8. Partial ^1H - ^1H COSY NMR spectrum of **Ru-1** in CD_3CN .

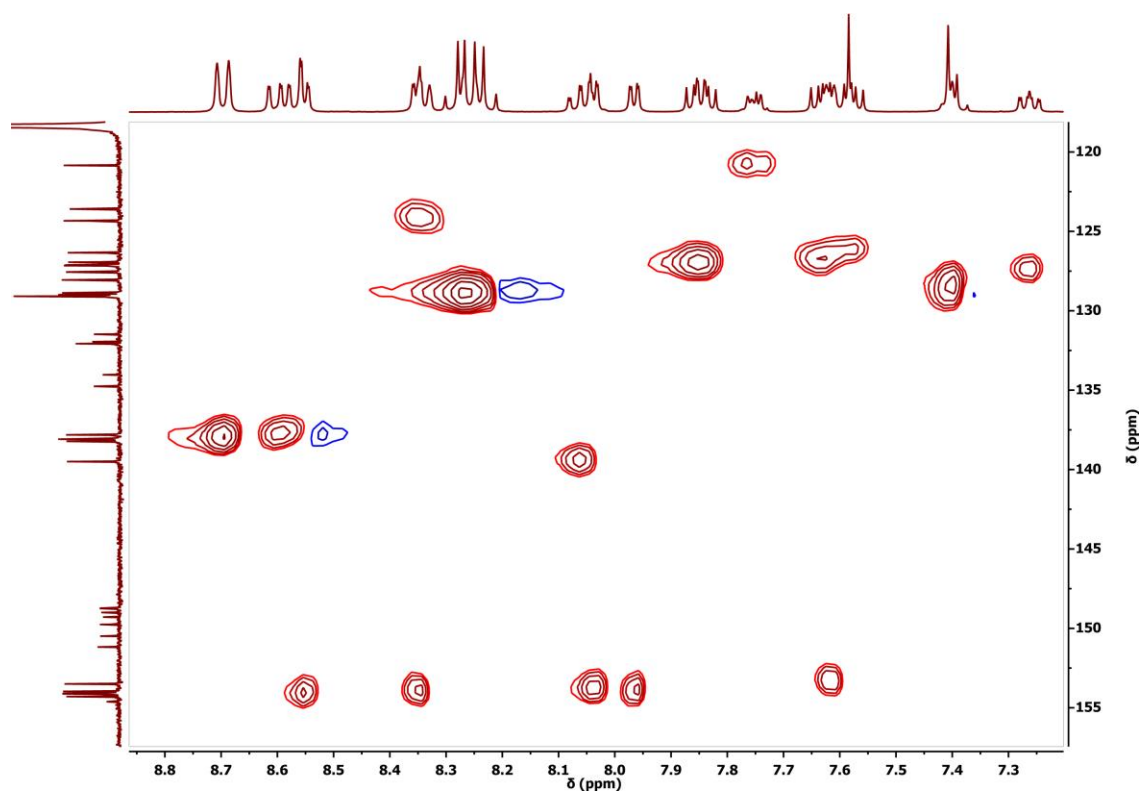


Figure S9. Partial ^1H - ^{13}C HSQC NMR spectrum of **Ru-1** in CD_3CN .

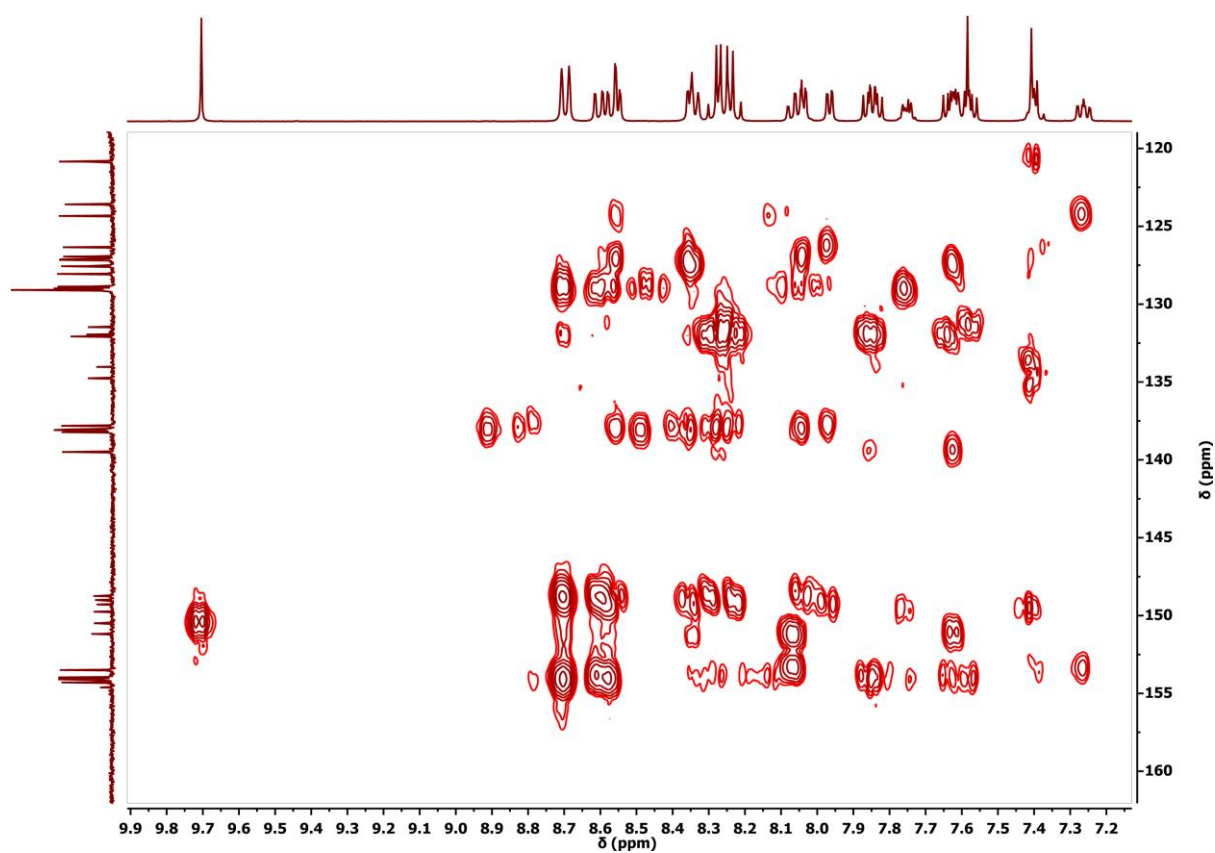


Figure S10. Partial ^1H - ^{13}C HMBC NMR spectrum of **Ru-1** in CD_3CN .

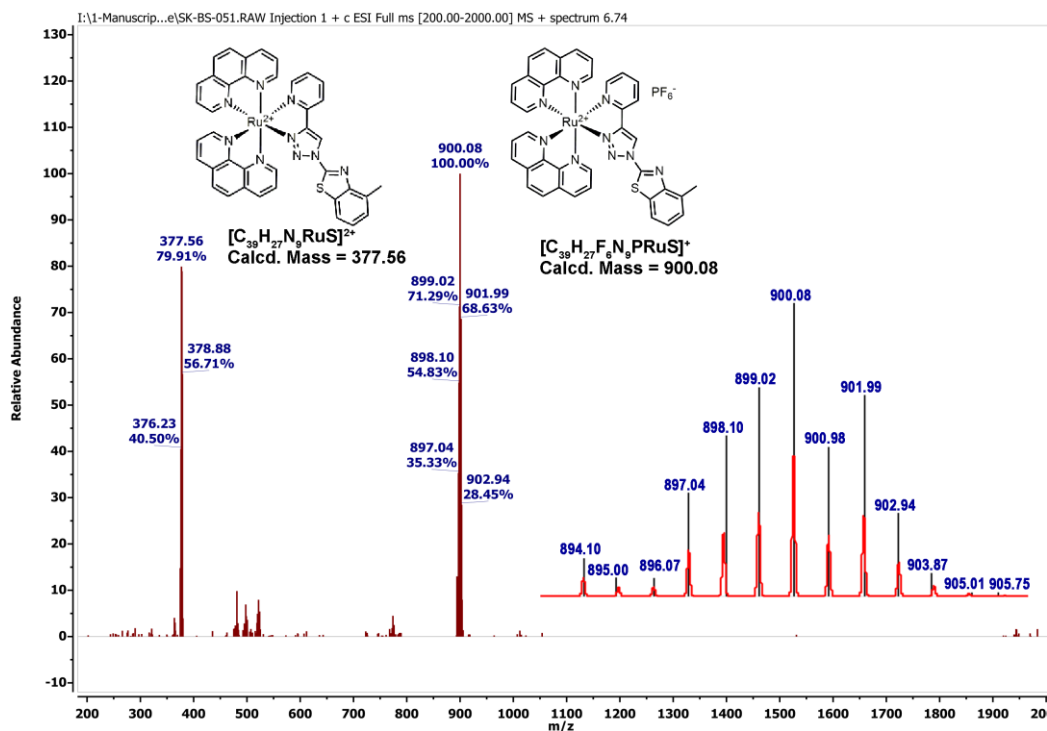


Figure S11. ESI mass spectrum of **Ru-1** in CH_3CN . Experimentally obtained (black), simulated (red).

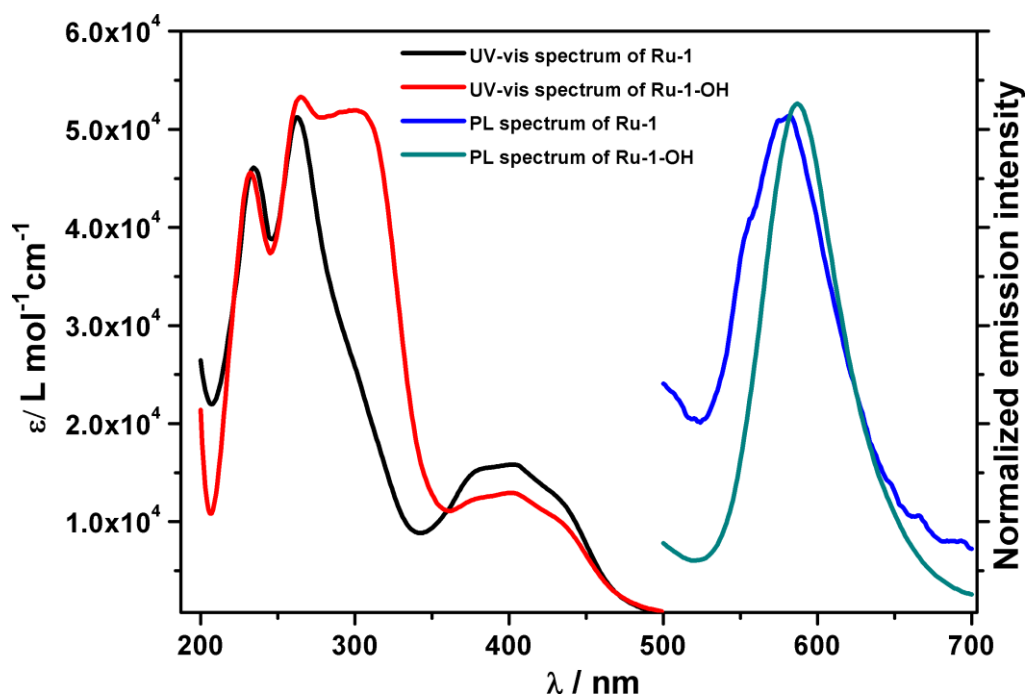


Figure S12. Normalized absorbance and PL spectra of **Ru-1** and **Ru-1-OH** (50 μM) in PBS buffer (PBS: DMSO = 9.5:0.5, v/v, pH 7.4). [$\lambda_{\text{ex}} = 400 \text{ nm}$; λ_{em} of **Ru-1** = $\sim 580 \text{ nm}$ and **Ru-1-OH** = $\sim 587 \text{ nm}$].

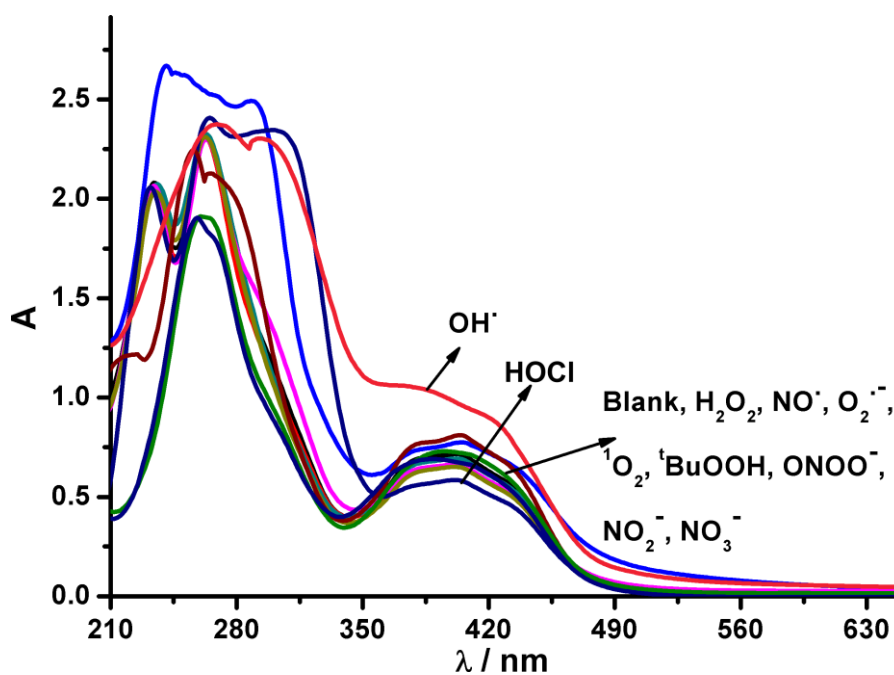


Figure S13. UV-vis selectivity of **Ru-1**(50 μ M) with HOCl (1.0 mM) and other ROS/RNS (10 mM) in PBS buffer ((PBS: DMSO = 9.5:0.5, v/v, pH 7.4).

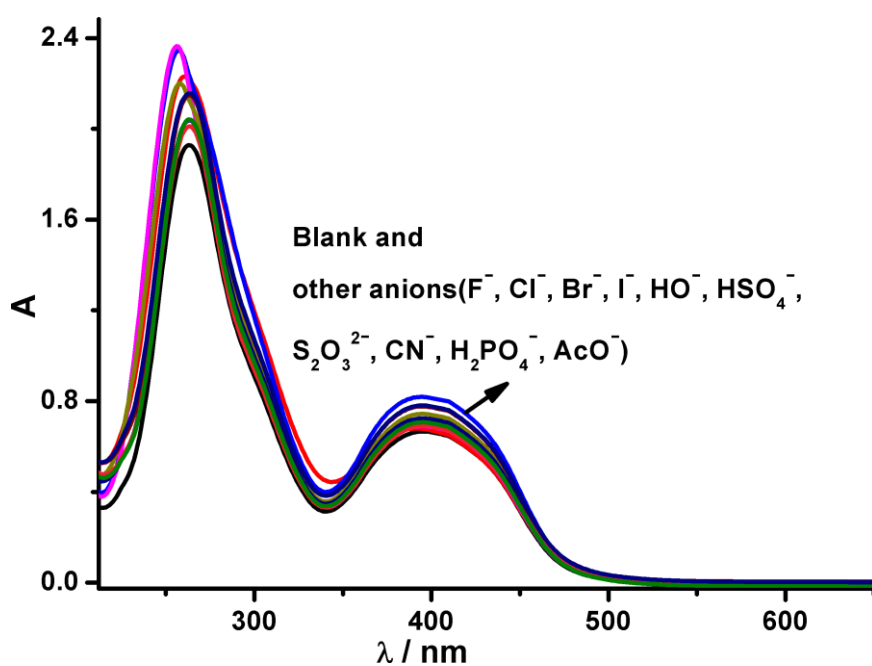


Figure S14. UV-vis selectivity of **Ru-1**(50 μ M) with HOCl (1.0 mM), anions (10.0 mM) in PBS buffer (PBS: DMSO = 9.5:0.5, v/v, pH 7.4).

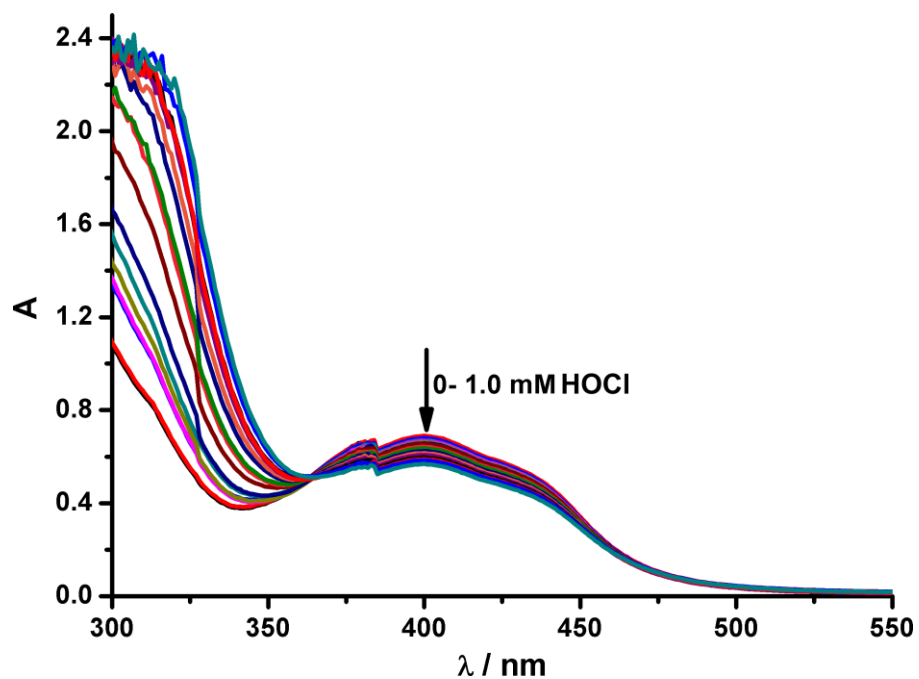


Figure S15. UV-vis titration of **Ru-1** (50 μM) with HOCl (0-1.0 mM) in PBS buffer (PBS: DMSO = 9.5:0.5, v/v, pH 7.4).

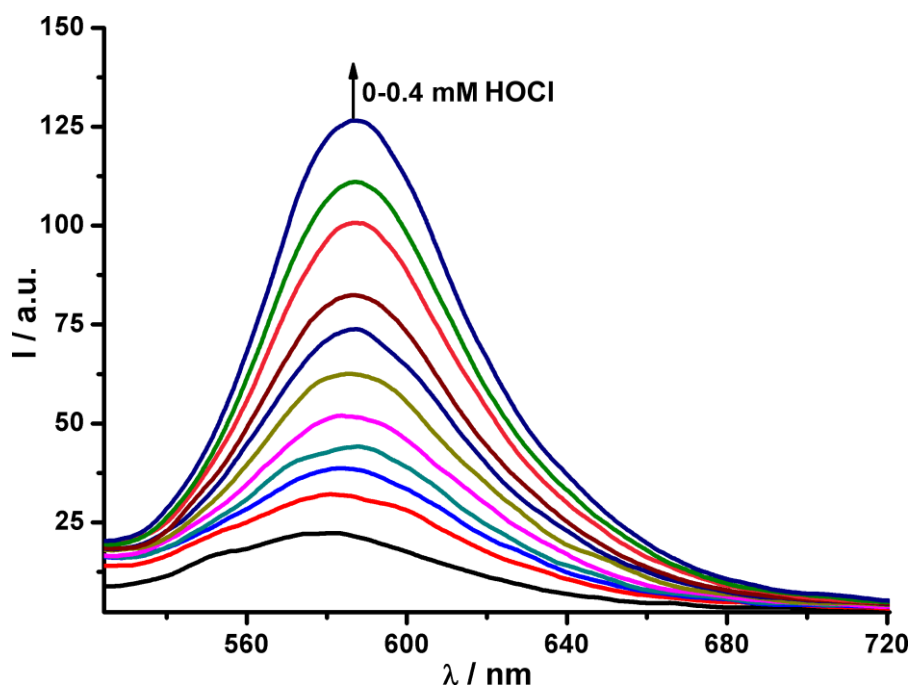


Figure S16. PL titration of **Ru-1** in the presence of HOCl (0-0.4 mM) for calculation of detection limit in PBS buffer (PBS: DMSO = 9.5:0.5, v/v, pH 7.4).

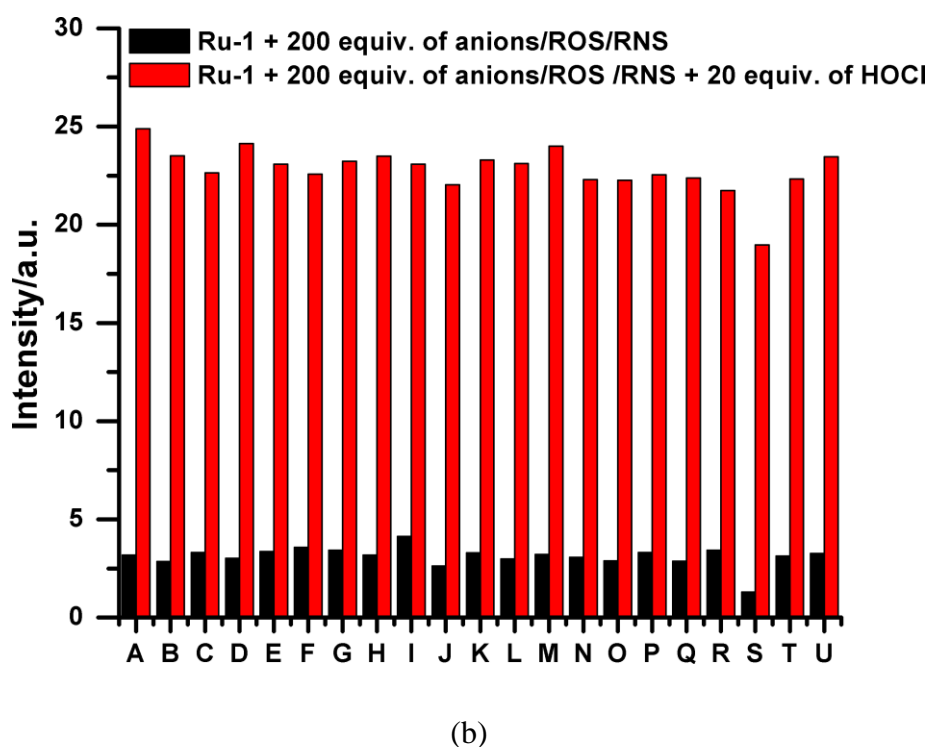
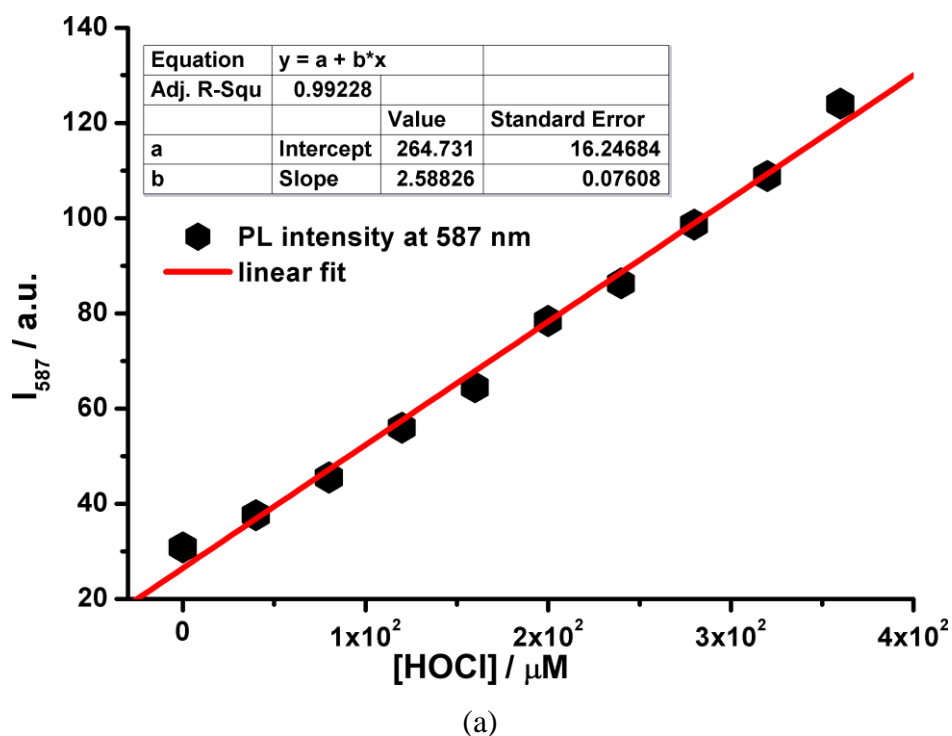


Figure S17. (a) PL intensity ($\lambda_{em} = 587$ nm) versus concentration of HOCl plot for calculation of the HOCl detection limit for **Ru-1**. (b) The PL response of **Ru-1** in the presence of competing analytes (200 equiv.) with 20 equiv. HOCl (red) and without HOCl (black). (A-U: blank, F^- , Cl^- , Br^- , I^- , AcO^- , OH^- , CN^- , HS^- , HSO_4^- , $S_2O_3^{2-}$, $H_2PO_4^-$, NO_2^- , NO_3^- , $ONOO^-$, H_2O_2 , NO^\cdot , $O_2^{\cdot-}$, $^{\cdot}OH$, 1O_2 , tBuOOH).

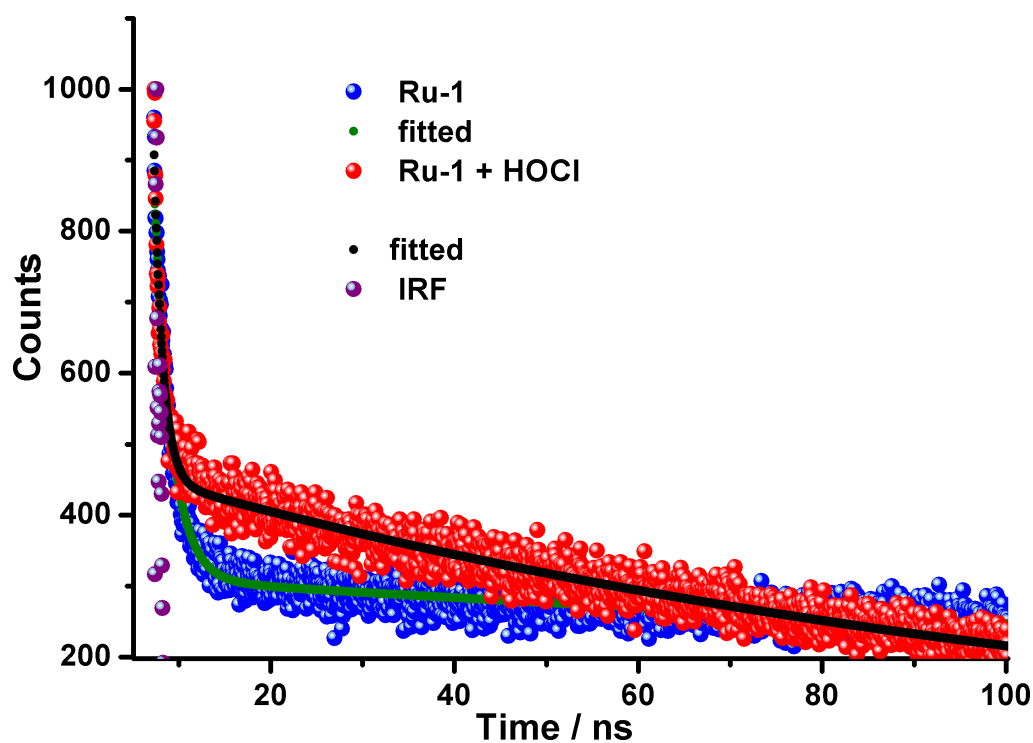


Figure S18. Time-resolved fluorescence spectra of **Ru-1** (50 μM) before and after addition of HOCl (1.0 mM) in aqueous PBS buffer-DMSO (9.5:0.5, v/v, pH 7.4) solution.

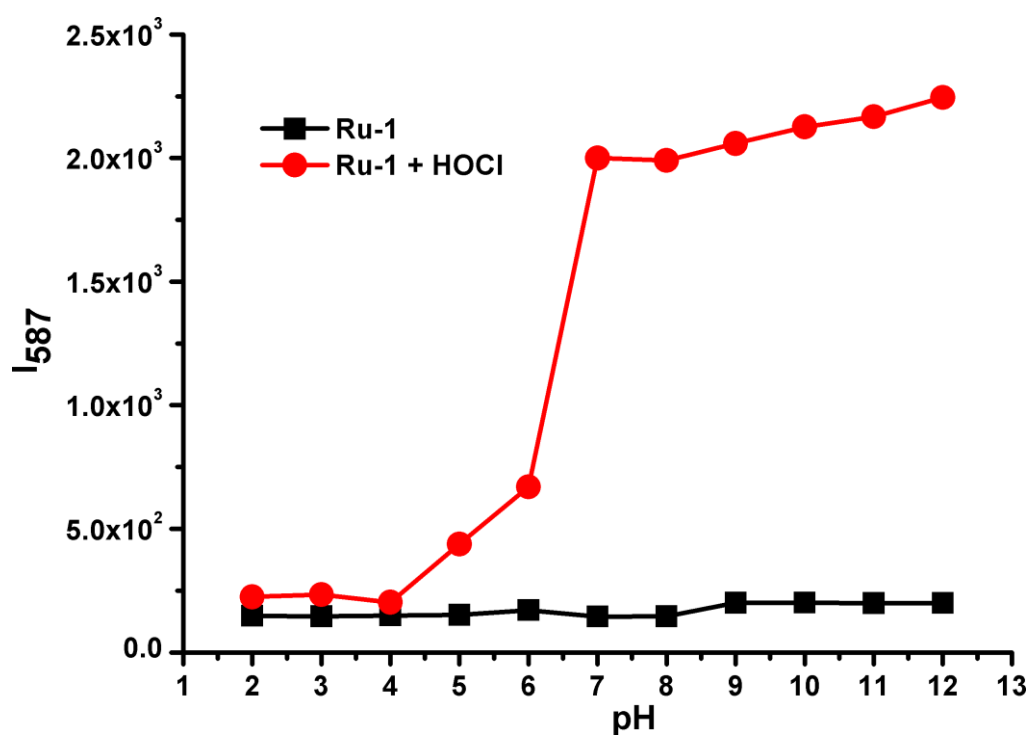


Figure S19. Effect of pH on luminescence intensity of **Ru-1**(50 μM) in the absence and presence of HOCl (1.0 mM).

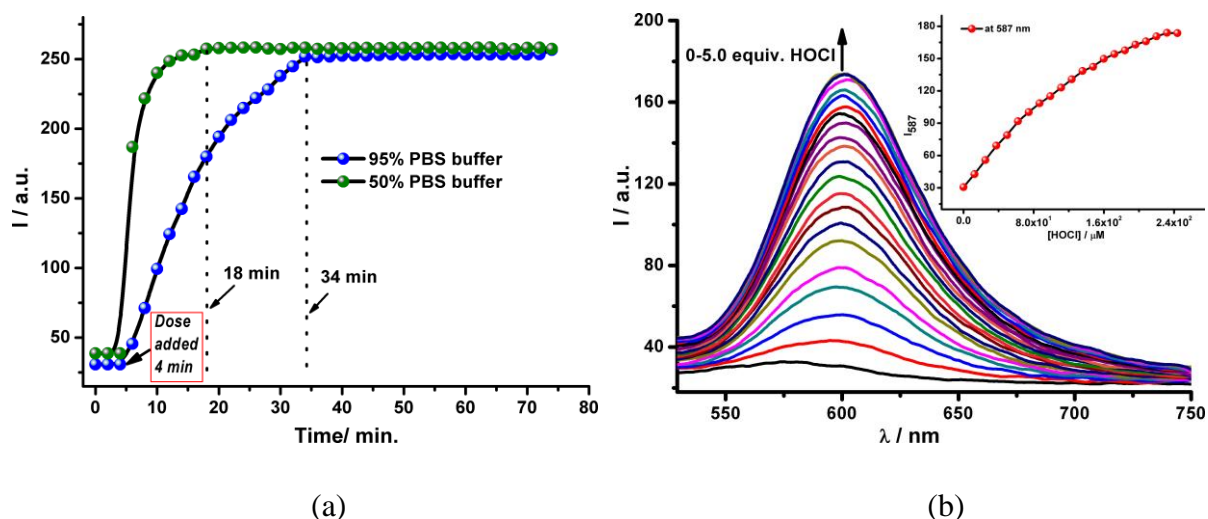


Figure S20. (a) PL intensity over time for **Ru-1** (50 μM) in the presence of HOCl (1.0 mM) in different percentage of DMSO/PBS (pH-7.4) mixture (v/v). (b) PL titration of **Ru-1** in the presence of HOCl (0-5 equiv.) in DMSO.

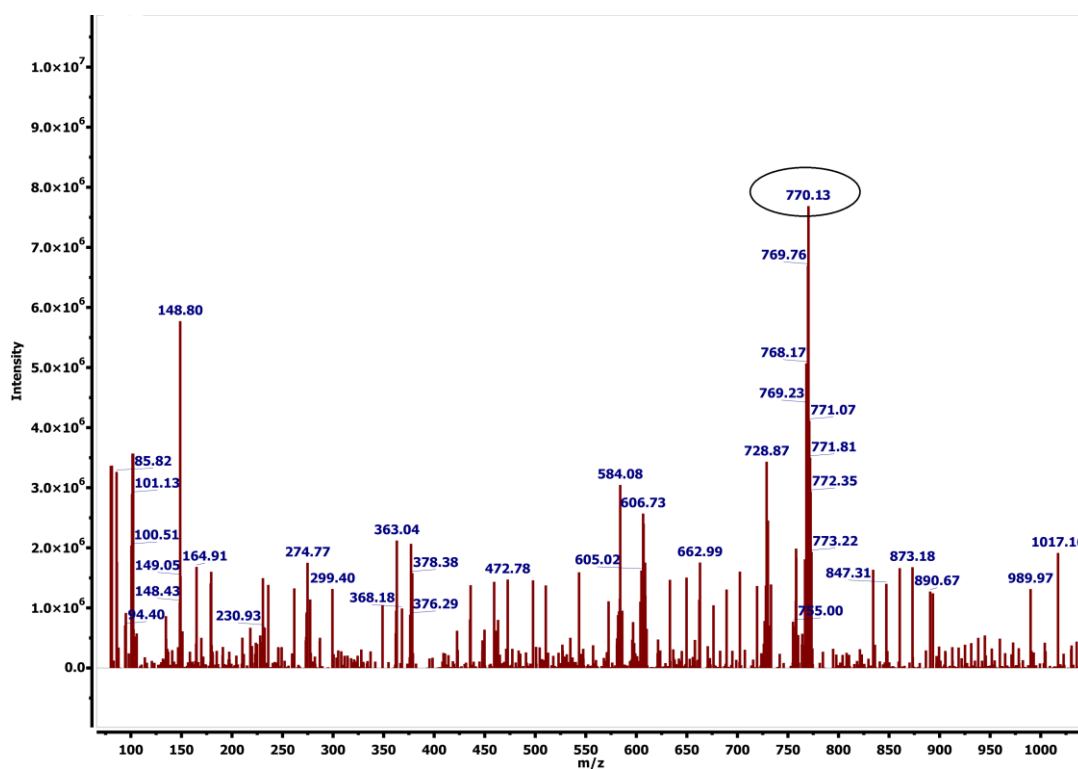


Figure S21. ESI mass spectrum of **Ru-1**(0.2 mM) reacted with 2.0 mM of NaOCl in CH₃CN.

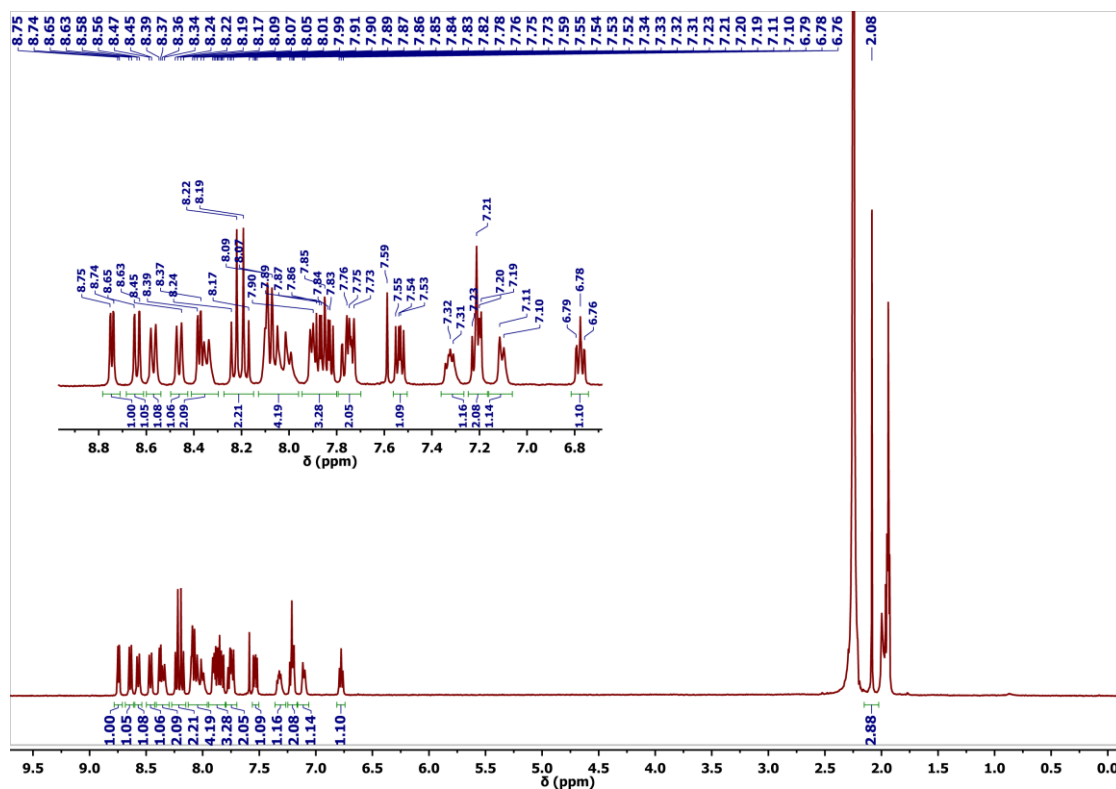


Figure S22. ¹H NMR spectrum of **Ru-1-OH** in CD₃CN (400 MHz).

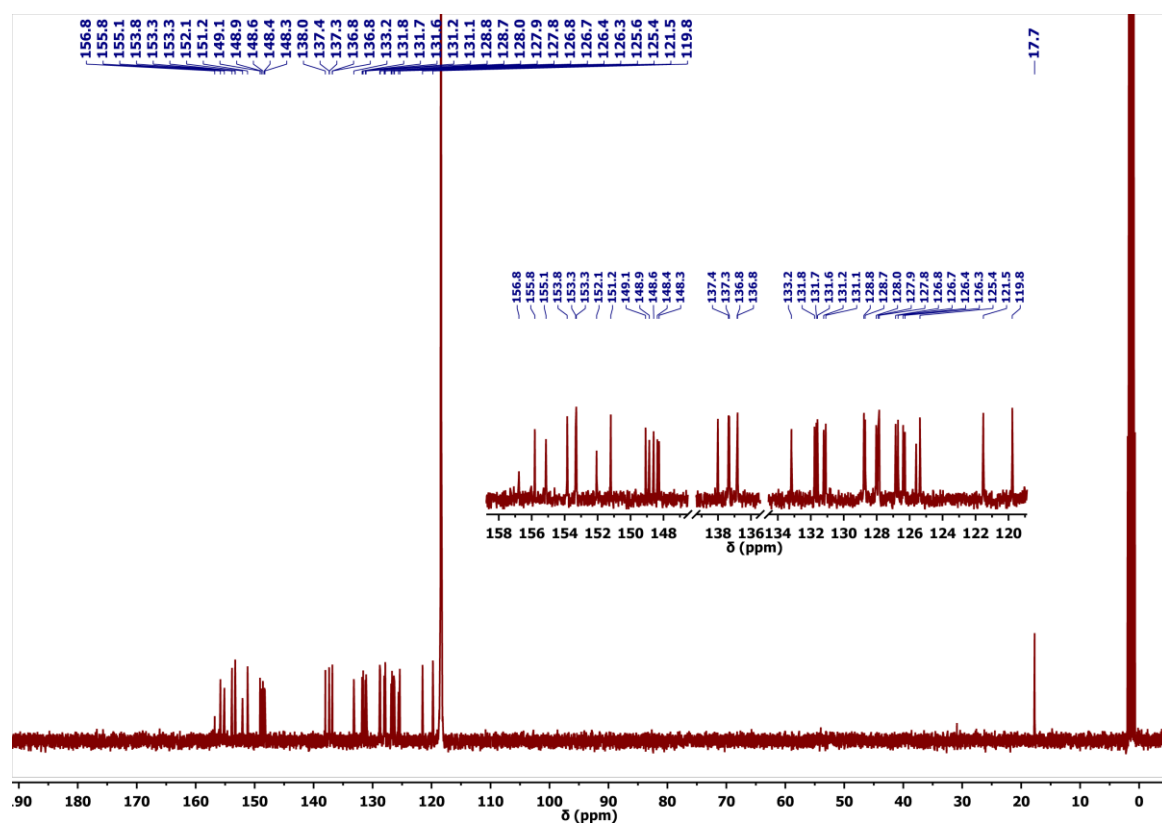


Figure S23. ¹³C NMR spectrum of **Ru-1-OH** in CD₃CN (100 MHz).

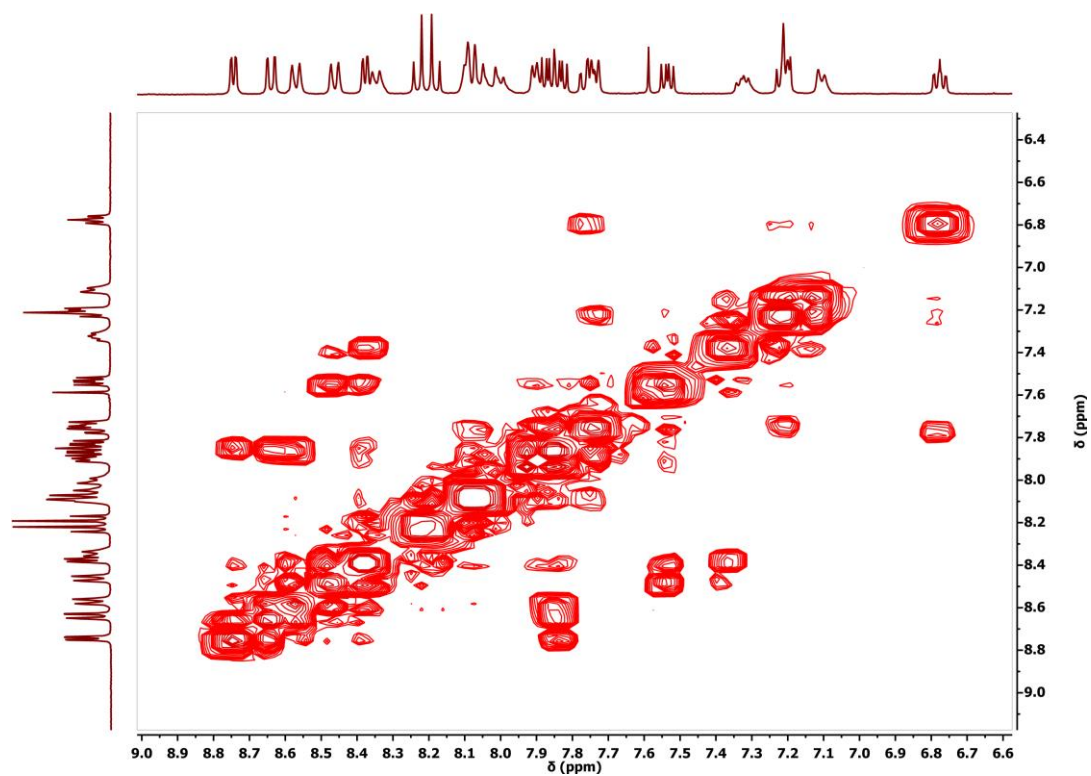


Figure S24. Partial ^1H - ^1H COSY NMR spectrum of **Ru-1-OH** in CD_3CN .

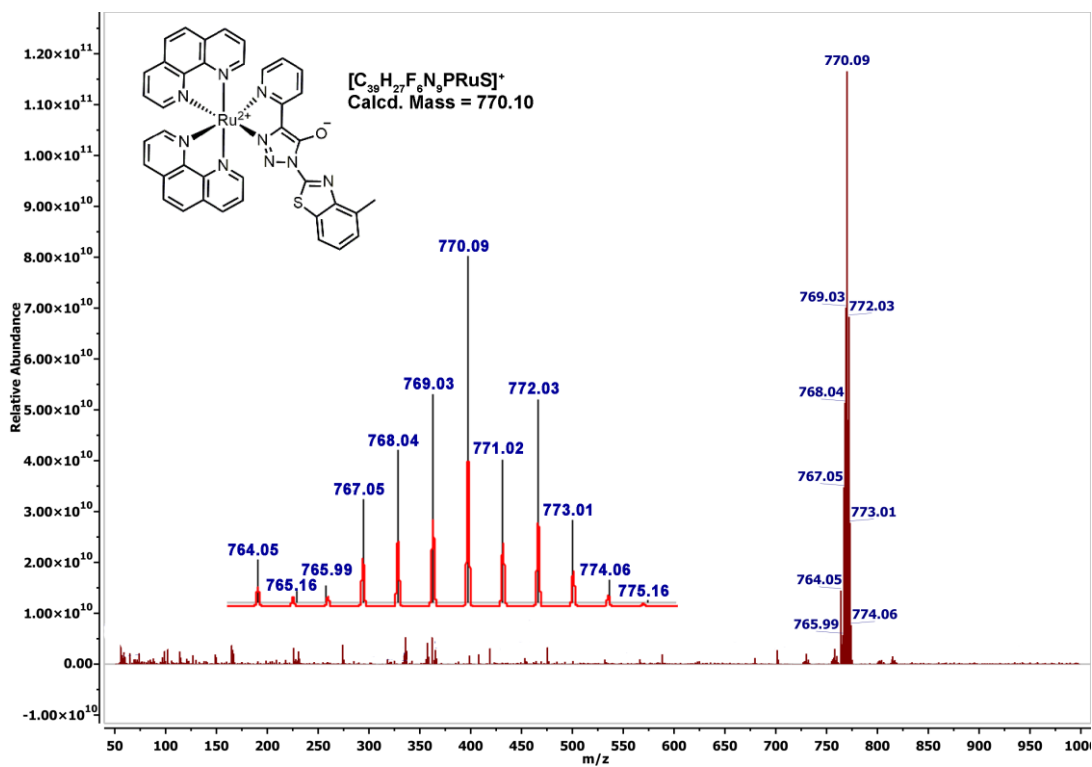


Figure S25. ESI mass spectrum of **Ru-1-OH** in CH_3CN . Experimentally obtained (black), simulated (red).

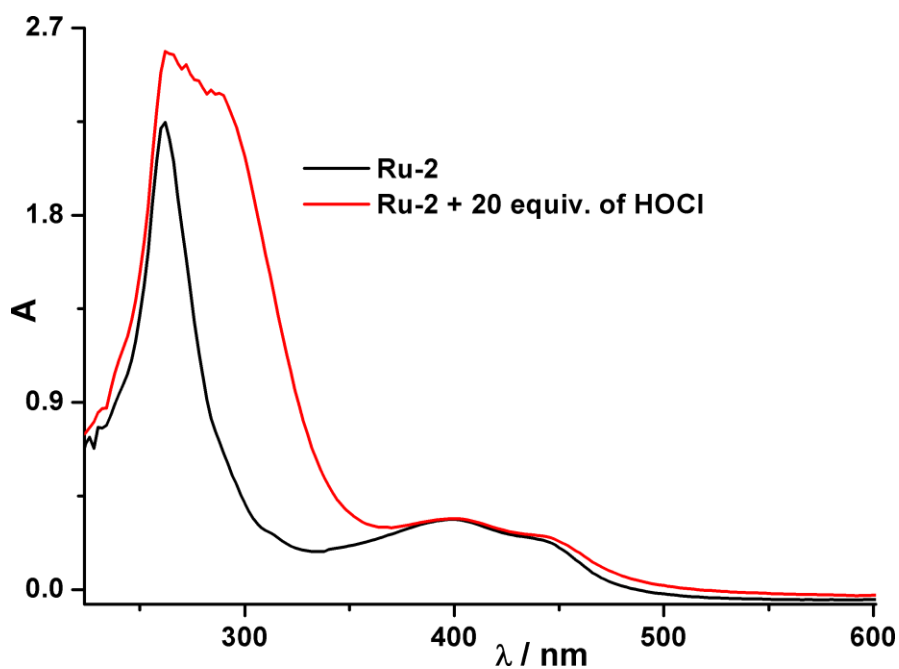


Figure S26. The UV-vis spectra of **Ru-2** (50 μ M) in the presence of 20 equiv. of HOCl in 75% DMSO-PBS buffer (pH=7.4).

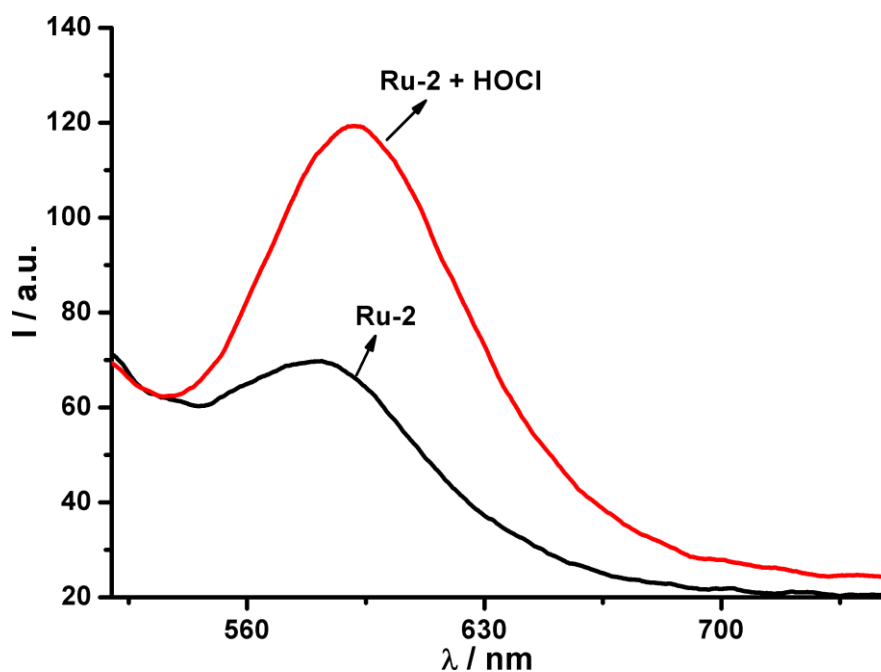


Figure S27. The PL spectra of **Ru-2** (50 μ M) in the presence of 20 equiv. of HOCl in 75% DMSO-PBS buffer (pH=7.4). (λ_{ex} = 403 nm, λ_{em} = 592 nm).

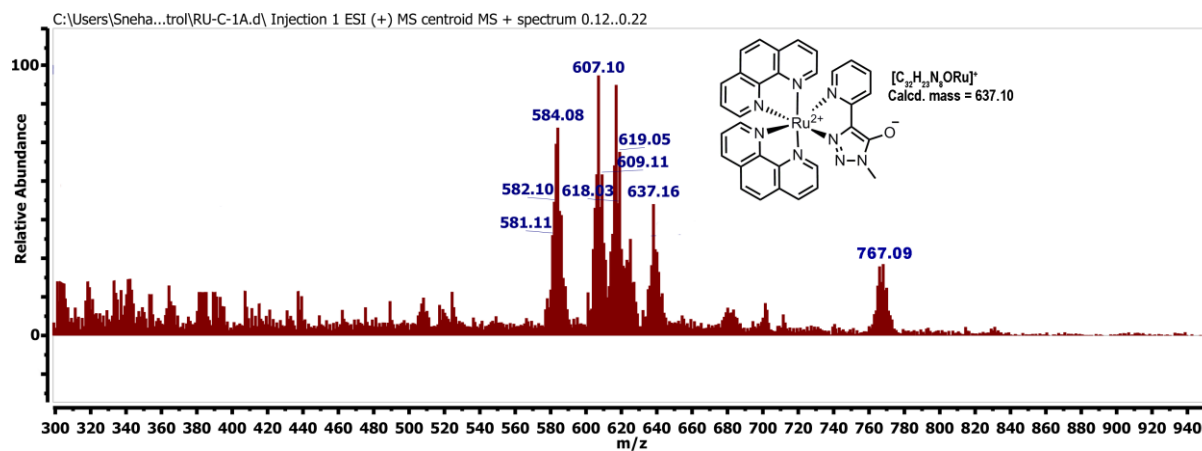


Figure S28. ESI mass spectrum of **Ru-2** in the presence of 10 equiv. of NaOCl in CH_3CN .

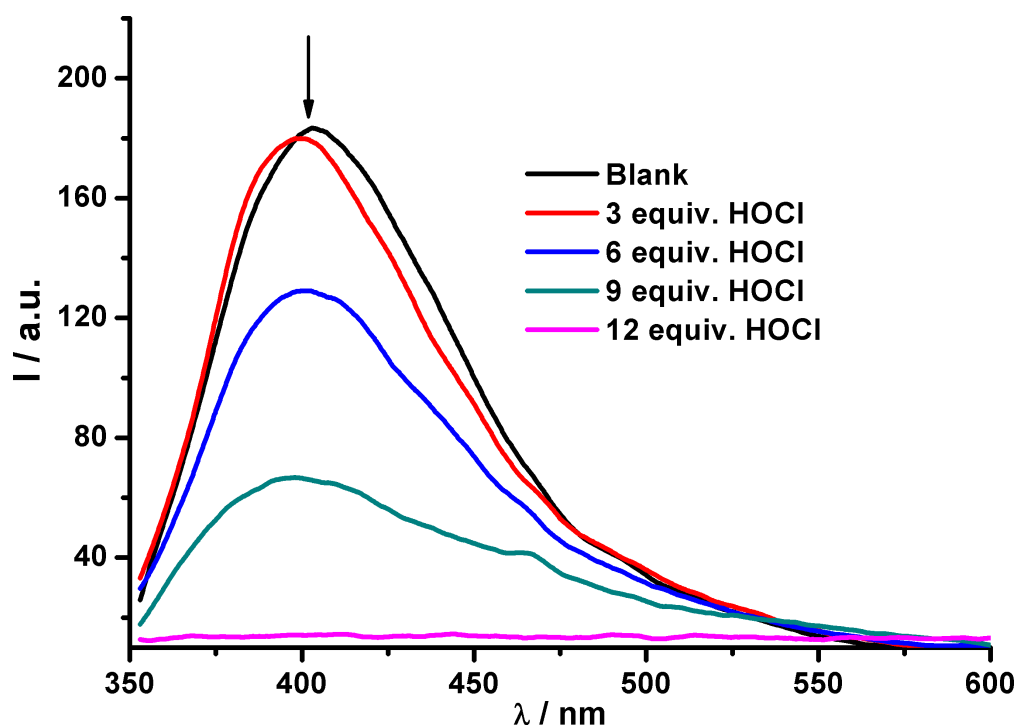


Figure S29. PL titration of **BtPT** (50 μM) in the presence of 0-12.0 equiv. of HOCl in 50% DMSO-PBS buffer (pH=7.4). (λ_{ex} = 309 nm, λ_{em} = 390 nm).

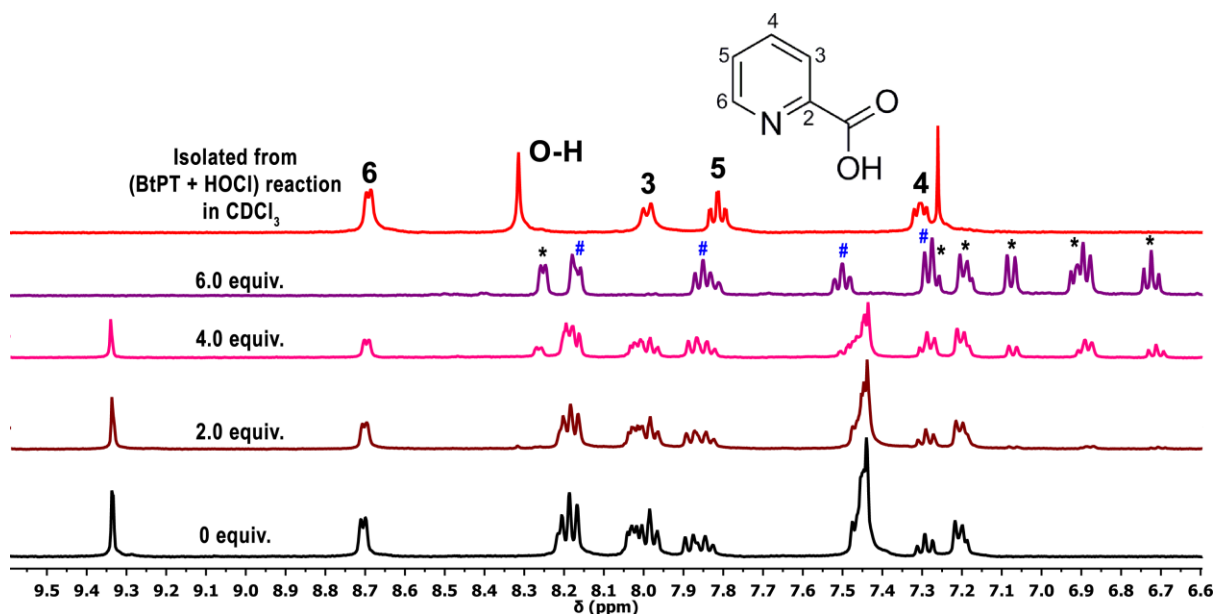


Figure S30. (a) Partial ^1H NMR spectra of isolated picolinic acid (**PA**) from **BtPT** and NaOCl (10.0 equiv.) reaction (red colour) and ^1H NMR titration spectra of **BtPT** ligand with NaOCl (0-6.0 equiv.) in $\text{DMSO}-d_6$ at room temperature (black to violet colour). The asterisks (*) and number sign (#) are showing the ^1H NMR signals of hydroxylated product of **BtPT** and picolinic acid (**PA**) protons respectively.

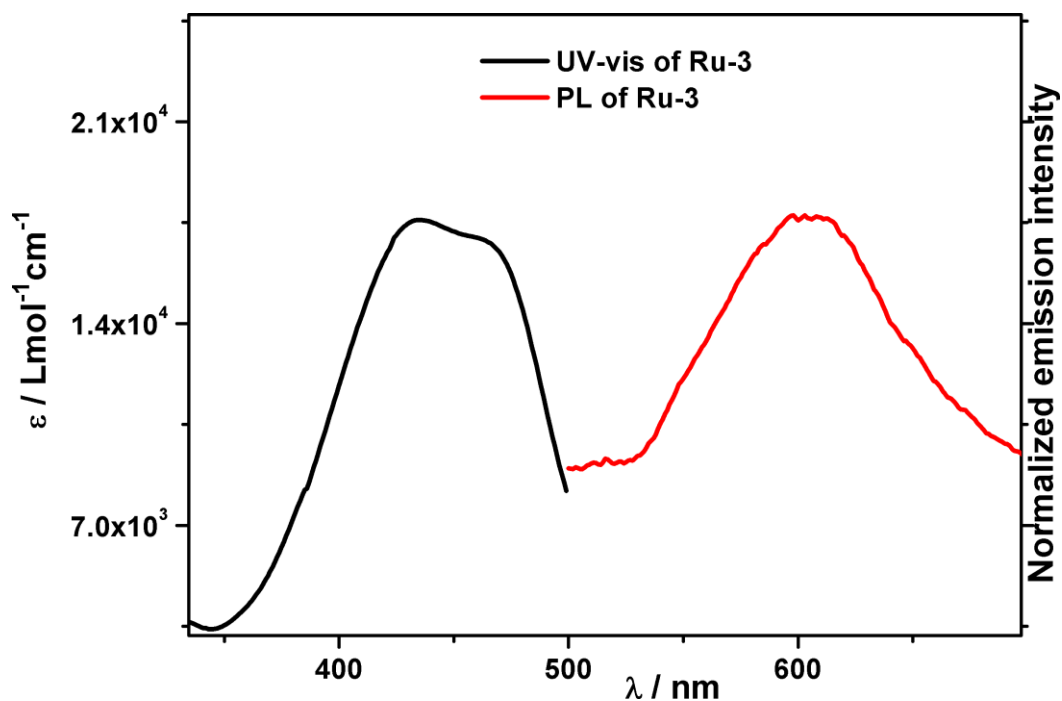


Figure S31. Normalized absorbance and PL spectra of **Ru-3** (50 μM) in PBS buffer (PBS: DMSO = 9.5:0.5, v/v, pH 7.4) ($\lambda_{\text{ex}} = 467$ nm, $\lambda_{\text{em}} = 606$ nm).

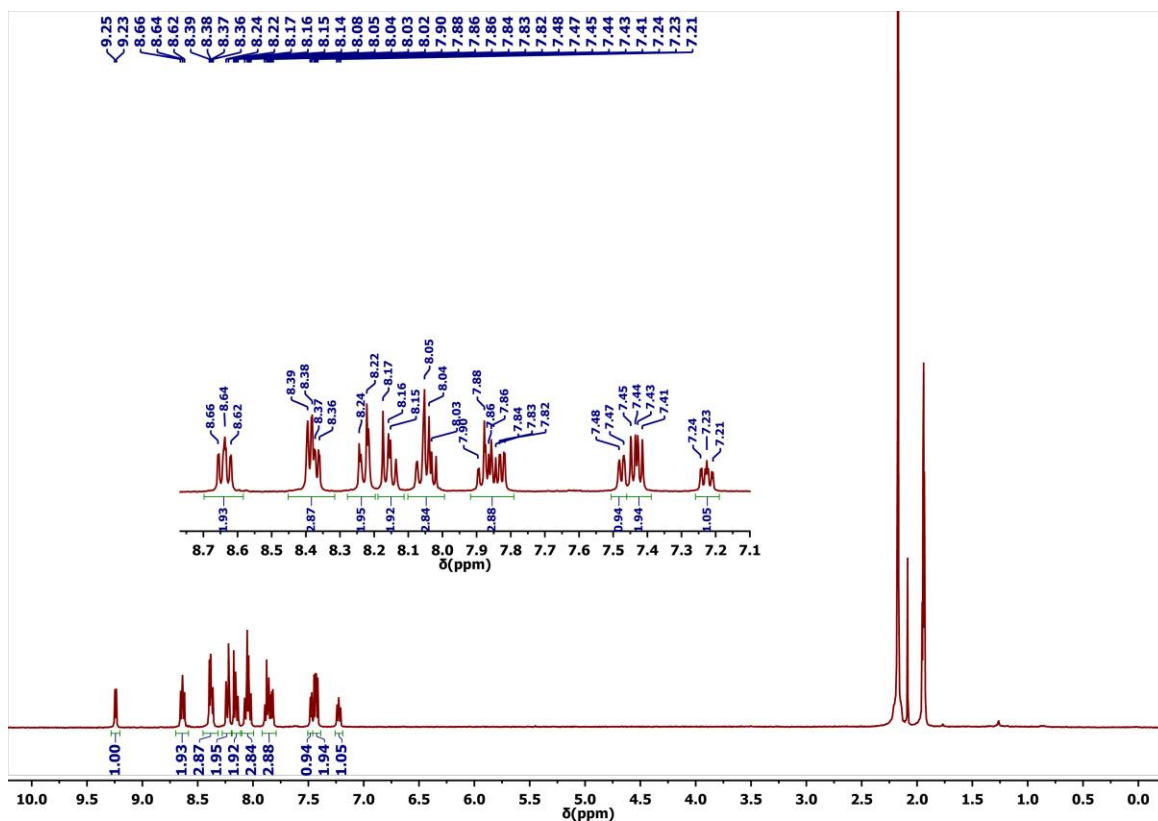


Figure S32. ¹H NMR spectrum of **Ru-3** in CD₃CN (400 MHz).

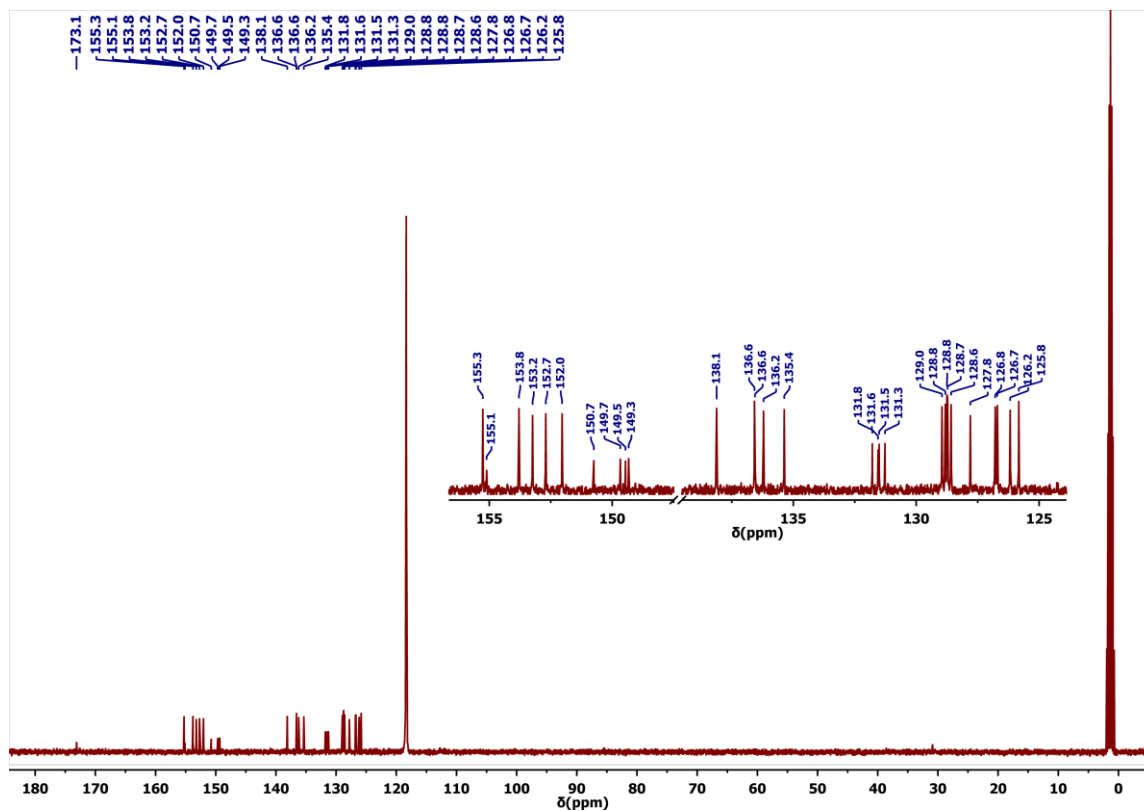


Figure S33. ¹³C NMR spectrum of **Ru-3** in CD₃CN (100 MHz).

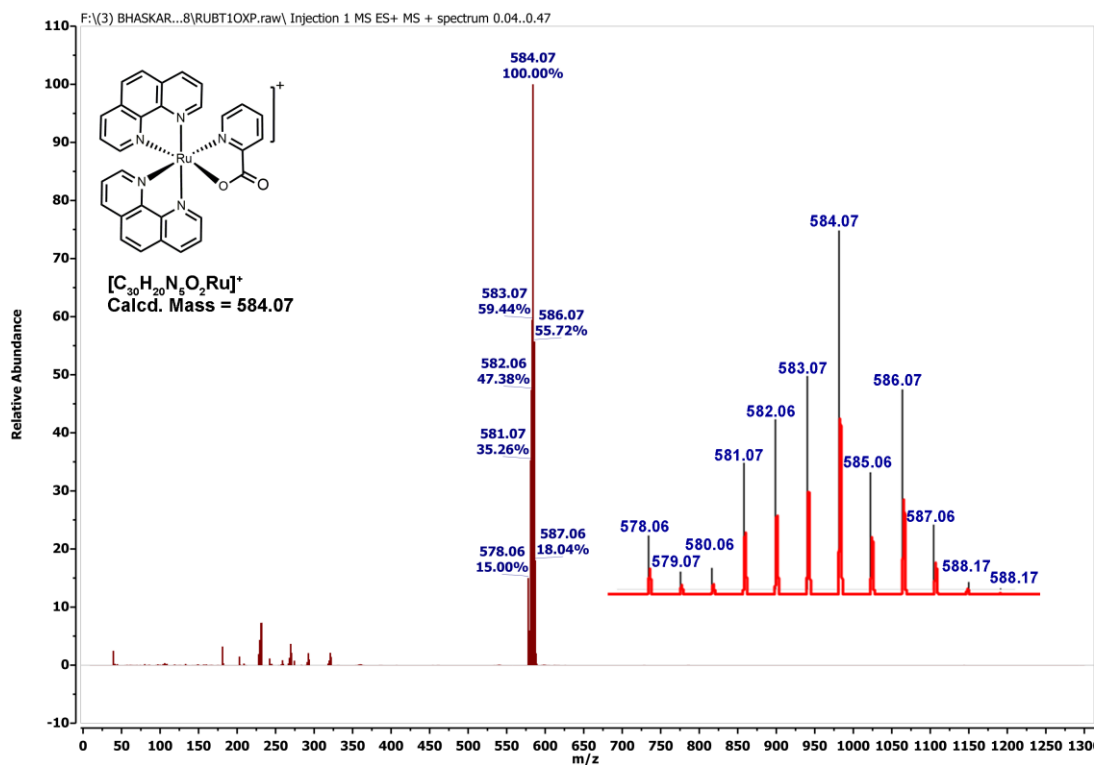


Figure S34. ESI mass spectrum of **Ru-3** in CH_3CN . Experimentally obtained (black), simulated (red).

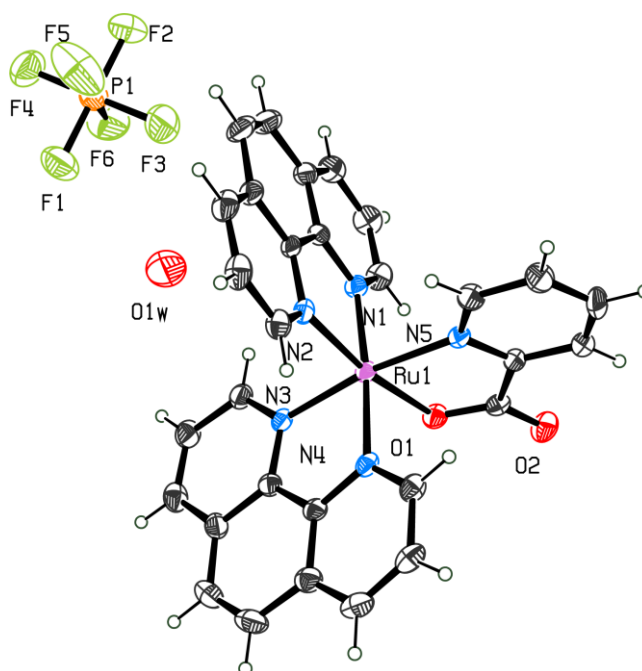
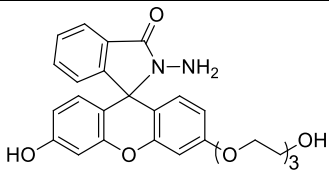
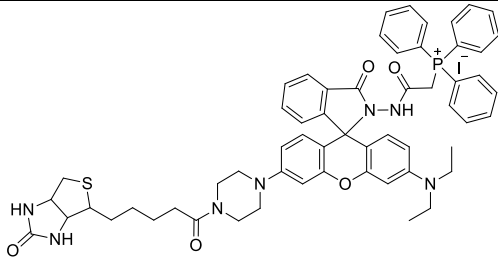
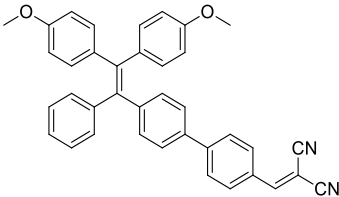
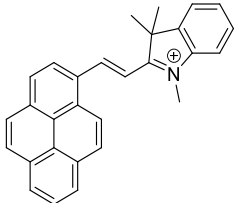
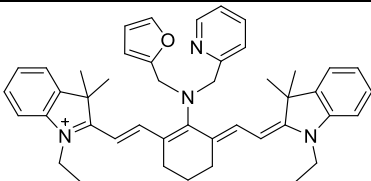
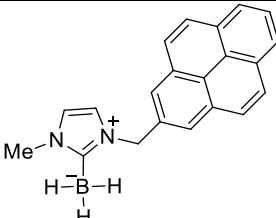
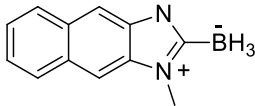
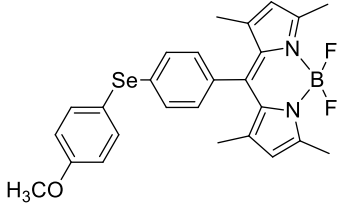
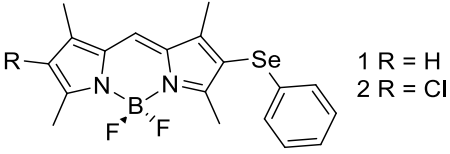
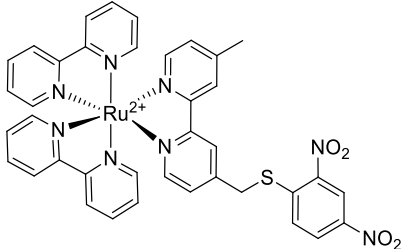
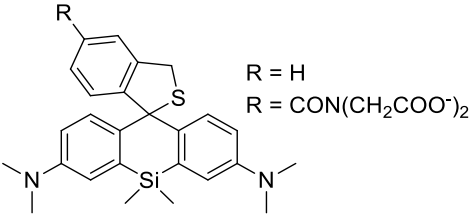
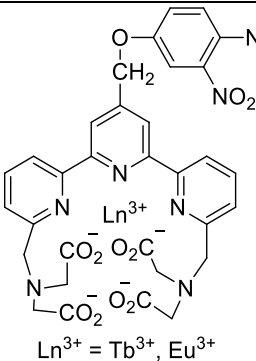
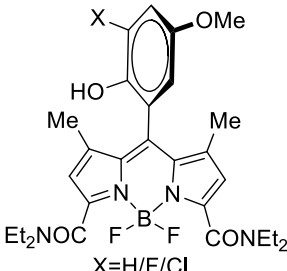
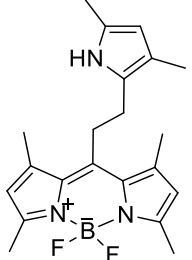


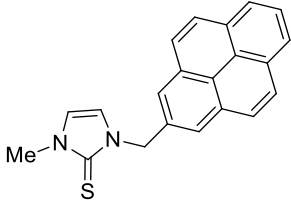
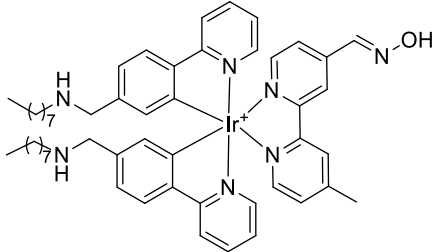
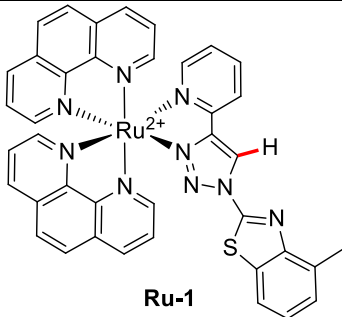
Figure S35. ORTEP^[8] plot of **Ru-3**· H_2O with 30% thermal ellipsoid probability. Only non-carbon and non-hydrogen atoms are labelled here.

4. List of selected probes for HClO/ClO⁻ detection

Table S1. List of selected probes based on spirolactam ring opening, oxidation of C=C bond, B-H bond, pyrrole ring, thione moiety, p-aminophenol, p-methoxyphenol, selenium, thioether, deoximation reaction and our probe, **Ru-1** for HClO/ClO⁻ detection.

Reference	Structure	ClO ⁻ mediated reaction for HOCl/ClO ⁻ sensing	Detection Limit (DL)
<i>J. Am. Chem. Soc.</i> 2016 , 138, 3769–3778		Spirolactam ring opening	Not reported
<i>Chem. Commun.</i> 2017 , 53, 5539–5541		Spirolactam ring opening	0.21 μM
<i>Chem. Commun.</i> , 2016 , 52, 7288–7291		Oxidation of C=C bond.	0.47 μM
<i>ACS Appl. Mater. Interfaces</i> 2016 , 8, 1511–1519		Oxidation of C=C bond	0.35 μM
<i>Anal. Chem.</i> 2014 , 86, 671–677		Oxidation of C=C bond	0.13 and 0.70 μM
<i>Angew. Chem. Int. Ed.</i> 2018 , 57, 1567 – 1571		Oxidation of B-H bonds	3 μM
<i>Anal. Chem.</i> 2018 , 90, 12937–12943		Oxidation of B-H bonds	3.6 μM

<i>Chem. Commun.</i> 2013 , 49, 1014–1016		Oxidation of selenium to selenoxide	Not reported
<i>Chem. Eur. J.</i> 2016 , 22, 1 – 8	 1 R = H 2 R = Cl	Oxidation of selenium to selenoxide	30.9 nM for 1 and 4.5 nM for 2
<i>Inorg. Chem.</i> 2013 , 52, 10325–10331		Oxidation of benzylthioether linker.	53.5 nM
<i>J. Am. Chem. Soc.</i> 2011 , 133, 5680–5682	 R = H R = CON(CH ₂ COO ⁻) ₂	Oxidation of thioether to sulfonate	Not reported
<i>Anal. Chem.</i> 2012 , 84, 10785–10792	 Ln ³⁺ = Tb ³⁺ , Eu ³⁺	Oxidation of p-aminophenol	1.3 nM and 0.64 nM
<i>Org. Lett.</i> 2014 , 16, 3544–3547	 X = H/F/Cl	Oxidation of p-methoxyphenol to benzoquinone	42, 18, and 37 nM
<i>J. Am. Chem. Soc.</i> 2014 , 136, 12820–12823		Oxidation of Pyrrole ring	0.56 nM

<i>Anal. Chem.</i> 2018 , 90, 9510–9514		Oxidation of thione moiety	0.2 μM
<i>Chem. Sci.</i> 2018 , 9, 7236–7240		Deoximation reaction	Not reported
Present work	 Ru-1	C(sp ²)-H hydroxylation	76 nM

NB: DL value in **bold** is above our probe **Ru-1**.

5. X-ray Crystallography

The X-ray data of **Ru-1** and **Ru-3** were collected at 293 K with Agilent Xcalibur (Eos, Gemini) diffractometer using graphite-monochromated Mo K α radiation ($\lambda = 0.71073$ Å). For both complex the data was collected, reduced and cell refinement was done in CrysAlis PRO (Agilent, 2013) software.^[9] For both the complexes, **Ru-1**•2CHCl₃ and **Ru-3**•H₂O, the absorption was corrected by SCALE3 ABSPACK multi-scan method in CrysAlisPro. The structures of **Ru-1**•2CHCl₃ and **Ru-3**•H₂O were solved by direct methods using the program SHELXS-97^[10] and SIR92^[11] respectively and refined by full matrix least-squares calculations (F^2) by using the SHELXL-2014/2017 software^[12] within the WinGX^[13] environment. All non-H atoms were refined anisotropically against F^2 for all reflections. All hydrogen atoms were placed at their calculated positions and refined isotropically. Crystal data collection and refinement details, selected bond lengths and angles for **Ru-1**•2CHCl₃ and **Ru-3**•H₂O are given in Table S2 to Table S4 respectively. The .cif file was deposited with the Cambridge Crystallographic Data Centre, and the following code was allocated: CCDC- 1497233, and 1831199 for **Ru-1**•2CHCl₃ and **Ru-3**•H₂O respectively. This data can be obtained free of charge via the Internet: [www.ccdc.cam.ac.uk/ data_request/cif](http://www.ccdc.cam.ac.uk/data_request/cif).

Table S2. Crystal data and structure refinement for **Ru-1•2CHCl₃**

Empirical formula	C ₄₁ H ₂₉ Cl ₆ F ₁₂ N ₉ P ₂ RuS	
Formula weight	1283.50	
Temperature	293(2) K	
Wavelength	0.71073 Å	
Crystal system	Triclinic	
Space group	<i>P</i> -1	
Unit cell dimensions	<i>a</i> = 12.172(5) Å	<i>α</i> = 85.132(5)°
	<i>b</i> = 13.741(5) Å	<i>β</i> = 80.312(5)°
	<i>c</i> = 15.292(5) Å	<i>γ</i> = 87.528(5)°
Volume	2511.0(16) Å ³	
Z	2	
Density (calculated)	1.698 Mg/m ³	
Absorption coefficient	0.824 mm ⁻¹	
Crystal size	0.150 x 0.120 x 0.090 mm ³	
F(000)	1276	
Theta range for data collection	3.172 to 28.984°	
Reflections collected	17670	
Independent reflections	11347 [<i>R</i> (int) = 0.0359]	
Completeness to theta = 25.242°	99.5 %	
Absorption correction	Semi-empirical from equivalents	
Max. and min. transmission	0.930 and 0.886	
Refinement method	Full-matrix least-squares on F ²	
Data / restraints / parameters	11347 / 0 / 650	
Goodness-of-fit on F ²	1.019	
Final <i>R</i> indices [<i>I</i> > 2σ(<i>I</i>)] ^a	<i>R</i> ₁ = 0.0796, <i>wR</i> ₂ = 0.2161	
<i>R</i> indices (all data) ^a	<i>R</i> ₁ = 0.1151, <i>wR</i> ₂ = 0.2466	
Largest diff. peak and hole	1.199 and -1.044 e.Å ⁻³	

^a *R*₁ = Σ||*F*_o| - |*F*_c||/Σ|*F*_o|; *wR*₂ = {Σ[*w*(*F*_o² - *F*_c²)²]/Σ*w*(*F*_o²)²}^{1/2}

Table S3. Selected Bond Lengths (Å) and Angles (°) around the Ru(II) center in **Ru-1•2CHCl₃** and **Ru-3•H₂O**

Ru-1•2CHCl₃			
Bond lengths (Å)			
N(1)-Ru(1)	2.066(5)	N(2)-Ru(1)	2.062(5)
N(3)-Ru(1)	2.065(4)	N(4)-Ru(1)	2.069(4)
N(5)-Ru(1)	2.090(5)	N(6)-Ru(1)	2.035(4)
Bond angles (°)			
N(6)-Ru(1)-N(2)	94.87(18)	N(6)-Ru(1)-N(3)	170.69(18)
N(2)-Ru(1)-N(3)	92.24(17)	N(6)-Ru(1)-N(1)	92.56(17)
N(2)-Ru(1)-N(1)	80.06(18)	N(3)-Ru(1)-N(1)	94.58(17)
N(6)-Ru(1)-N(4)	93.52(18)	N(2)-Ru(1)-N(4)	95.11(17)
N(3)-Ru(1)-N(4)	79.86(17)	N(1)-Ru(1)-N(4)	172.54(17)
N(6)-Ru(1)-N(5)	78.42(19)	N(2)-Ru(1)-N(5)	171.25(17)
N(3)-Ru(1)-N(5)	95.04(19)	N(1)-Ru(1)-N(5)	94.5(2)
N(4)-Ru(1)-N(5)	90.9(2)		

Ru-3•H₂O			
Bond lengths (Å)			
N(1)-Ru(1)	2.059(5)	N(2)-Ru(1)	2.048(3)
N(3)-Ru(1)	2.058(5)	N(4)-Ru(1)	2.070(5)
N(5)-Ru(1)	2.052(5)	O(1)-Ru(1)	2.099(3)
Bond angles (°)			
N(2)-Ru(1)-N(5)	94.88(18)	N(2)-Ru(1)-N(3)	91.49(17)
N(5)-Ru(1)-N(3)	171.26(16)	N(2)-Ru(1)-N(1)	80.40(18)
N(5)-Ru(1)-N(1)	92.02(18)	N(3)-Ru(1)-N(1)	94.94(18)
N(2)-Ru(1)-N(4)	99.10(18)	N(5)-Ru(1)-N(4)	93.47(18)
N(3)-Ru(1)-N(4)	79.59(17)	N(1)-Ru(1)-N(4)	174.51(18)
N(2)-Ru(1)-O(1)	170.67(14)	N(5)-Ru(1)-O(1)	79.19(17)
N(3)-Ru(1)-O(1)	95.20(16)	N(1)-Ru(1)-O(1)	92.53(17)
N(4)-Ru(1)-O(1)	88.51(16)		

Table S4. Crystal data and structure refinement for **Ru-3•H₂O**

Empirical formula	C ₃₀ H ₂₂ F ₆ N ₅ O ₃ PRu
Formula weight	744.56
Temperature	293(2) K
Wavelength	0.71073 Å
Crystal system	Orthorhombic
Space group	<i>P</i> n a 2 ₁
Unit cell dimensions	a = 10.4998(6) Å α = 90° b = 26.3329(11) Å β = 90° c = 10.3861(4) Å γ = 90°
Volume	2871.7(2) Å ³
Z	4
Density (calculated)	1.727 Mg/m ³
Absorption coefficient	0.684 mm ⁻¹
F(000)	1496
Crystal size	0.280 x 0.190 x 0.120 mm ³
Theta range for data collection	3.039 to 28.813°
Reflections collected	8538
Independent reflections	4516 [<i>R</i> (int) = 0.0318]
Completeness to theta = 25.000°	99.8 %
Absorption correction	Semi-empirical from equivalents
Max. and min. transmission	0.922 and 0.832
Refinement method	Full-matrix least-squares on <i>F</i> ²
Data / restraints / parameters	4516 / 1 / 415
Goodness-of-fit on <i>F</i> ²	1.021
Final <i>R</i> indices [<i>I</i> > 2σ(<i>I</i>)] ^a	<i>R</i> 1 = 0.0339, <i>wR</i> 2 = 0.0759
<i>R</i> indices (all data) ^a	<i>R</i> 1 = 0.0441, <i>wR</i> 2 = 0.0802
Absolute structure parameter	-0.05(2)
Largest diff. peak and hole	0.360 and -0.362 e.Å ⁻³

^a *R*1 = Σ||*F*_o| - |*F*_c||/Σ|*F*_o|; *wR*2 = {Σ[*w*(*F*_o² - *F*_c²)²]/Σ*w*(*F*_o²)²}^{1/2}.

6. Computational Study.

Density functional theory (DFT) and time dependant-density functional theory (TD-DFT) calculations (Table S5-S10) were performed to obtain insight into the electronic transitions responsible for the absorption spectra and luminescence spectra of **Ru-1** and **Ru-1-OH**. It is expected that the **Ru-1-OH** in 95% aqueous buffer solution exists as enolate, so the deprotonated form, **Ru-1-O⁻** was used for all computation. The singlet state TD-DFT calculations in water reflect that the highest and lowest lying MOs present in both **Ru-1** (HOMO, HOMO-1, HOMO-2 and LUMO, LUMO+1, LUMO+2, LUMO+3) (Figure S39) and **Ru-1-O⁻** (HOMO, HOMO-1, HOMO-2, HOMO-3 and LUMO, LUMO+2, LUMO+3, LUMO+4) (Figure S40) contribute major impact on metal-to-ligand charge-transfer (¹MLCT) bands which were observed experimentally at $\lambda_{\text{max}} = 400$ and 433 nm. The HOMOs of **Ru-1** are mainly located on ruthenium(II) center, whereas, in **Ru-1-O⁻**, HOMOs are situated on ruthenium(II) and partially on hydroxylated **BtPT** ligand (HOMO, HOMO-1, HOMO-3) (Figure S41-S42). The unoccupied molecular orbitals, LUMO, LUMO+2 and LUMO+3 of **Ru-1** correspond to ancillary phen ligand, whereas LUMO+1 correspond to **BtPT** ligand. Similarly, in the case of hydroxylated product, **Ru-1-O⁻**, the three unoccupied orbitals, LUMO, LUMO+2, and LUMO+3 correspond to ancillary phen ligand (Figure S41-S42). The TD-DFT calculations for **Ru-1** indicate that the experimental ¹MLCT absorption band at ~400 nm (3.10 eV) arises from strong transitions characterized as HOMO-2→LUMO+1, HOMO-1→LUMO+1, HOMO-1→LUMO+2 and HOMO→LUMO+3 ($f = 0.20$) (380.15 nm, 3.26 eV). The low energy electronic absorption band at ~433 nm (2.86 eV) in the visible range are assigned to transitions HOMO-2→LUMO, HOMO-2→LUMO+1, HOMO-2→LUMO+2, HOMO→LUMO+2 and HOMO→LUMO+3 ($f = 0.12$) (397.60 nm, 3.12 eV) (Figure S41 and Table S8). In **Ru-1-O⁻**, the calculated strong transition at 385.9 nm (3.21 eV), which is due to the HOMO-3→LUMO+3, HOMO-2→LUMO+2 and HOMO-2→LUMO+3 transitions ($f = 0.15$), is assigned to the experimental absorption band at ~400 nm. Whereas, the experimental absorption band at ~433 nm corresponds to calculated HOMO-3→LUMO, HOMO-2→LUMO, HOMO-1→LUMO+2 and HOMO-1→LUMO+3 transitions (404.9 nm; 3.06 eV) (Table S9 and Figure S42). The optimized ground states geometries from DFT calculation shows that the highest occupied MOs of **Ru-1** (HOMO, HOMO-2) and **Ru-1-O⁻** (HOMO, HOMO-4) are mainly $d\pi L\pi$ and $\text{Ru}(dz^2)$ in character (Figure 6a, S36-S38). Whereas, the lowest lying MOs of **Ru-1** and **Ru-1-O⁻** are centred at the $L\pi^*$ orbital of phenanthroline ligand. After HOCl stimulated hydroxylation of **BtPT** ligand,

the metal based (dz^2) HOMO-4 (-8.35 eV) of **Ru-1-O⁻** is destabilized by 2.53 eV compared to dz^2 based HOMO-2 (-10.88 eV) of **Ru-1**. Whereas, the $d\sigma^*$ orbital of **Ru-1-O⁻** (LUMO+11; $E = -2.48$ eV) is destabilized compared to the $d\sigma^*$ orbital of **Ru-1** (LUMO+9; $E = -5.08$ eV). Additionally, in **Ru-1-O⁻**, the phenanthroline ligand based LUMO ($L\pi^*$) is destabilized by 2.17 eV which indicates stabilization of $^1\text{MLCT}$ and destabilization of ^1MC after HOCl promoted hydroxylation, inhibits the thermally accessible non-radiative deactivation between MLCT and MC states found in case of **Ru-1** (Figure 6a).

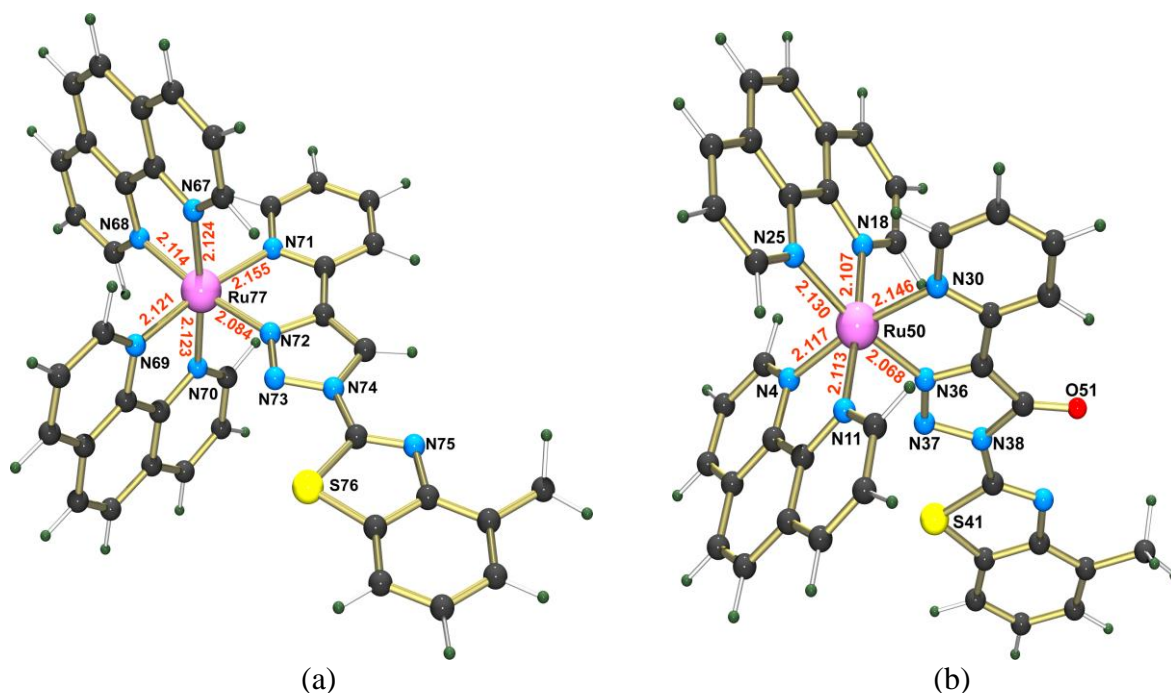


Figure S36. Optimized structure of (a) **Ru-1** and (b) **Ru-1-O⁻** in the ground state obtained from DFT calculations at B3LYP/6-31G (d,p) // LANL2DZ level.

Table S5. Selected Bond Lengths (Å) around the Ru(II) center in **Ru-1** and **Ru-1-O⁻** obtained from ground state DFT calculation.

Ru-1			
Bond lengths (Å)			
N(67)-Ru(77)	2.124	N(70)-Ru(77)	2.123
N(68)-Ru(77)	2.114	N(71)-Ru(77)	2.155
N(69)-Ru(77)	2.121	N(72)-Ru(77)	2.084
Ru-1-O⁻			
Bond lengths (Å)			
N(4)-Ru(50)	2.117	N(25)-Ru(50)	2.130
N(11)-Ru(50)	2.113	N(30)-Ru(50)	2.146
N(18)-Ru(50)	2.107	N(36)-Ru(50)	2.068

Table S6. Cartesian coordinates of **Ru-1** in the ground state

Ru-1							
	X	Y	Z		X	Y	Z
C	-2.41996	-2.19485	2.30236	H	-1.15199	0.44473	3.41701
H	3.3784	-1.75303	2.06742	C	-0.67265	2.53381	3.77952
C	-2.30889	-3.25159	3.20537	H	-0.63707	2.41829	4.85579
H	-3.19729	-3.64475	3.68391	C	-0.43408	3.76483	3.18576
C	-1.04411	-3.78723	3.47671	H	-0.2059	4.63646	3.78933
H	-0.93009	-4.60919	4.17342	C	-0.261	5.10874	1.06298
C	0.07203	-3.24759	2.83417	H	-0.02989	6.00198	1.6328
H	1.06282	-3.64352	3.02285	C	-0.33138	5.15679	-0.30258
C	-0.09774	-2.188	1.93686	H	-0.15604	6.08895	-0.82829
C	0.97938	-1.54702	1.20615	C	-0.72063	3.96661	-2.48758
C	2.35554	-1.68186	1.15016	H	-0.55152	4.87975	-3.04754
H	3.06324	-2.3208	1.64853	C	-1.01753	2.77913	-3.13914
C	4.08393	-0.4851	-0.17353	H	-1.08569	2.73818	-4.21915
C	6.20773	0.30816	-1.17536	C	-1.23182	1.60529	-2.39269
C	7.33078	0.83587	-1.80377	H	-1.45647	0.66684	-2.87982
H	7.25976	1.6379	-2.52803	C	-0.49008	3.87979	1.77531
C	8.56916	0.28331	-1.45964	C	-0.79137	2.70919	1.03342
H	9.46837	0.66773	-1.92811	C	-0.63638	3.98085	-1.07398
C	8.67291	-0.7592	-0.5201	C	-0.86607	2.76001	-0.39152
H	9.65257	-1.1589	-0.28223	C	-4.25792	0.99594	0.91137
C	7.5512	-1.29822	0.11799	H	-3.74842	1.62596	1.62761
C	6.29922	-0.74237	-0.22735	C	-5.65566	1.05193	0.756
C	7.65434	-2.41457	1.12474	H	-6.22787	1.74076	1.36512
H	8.69446	-2.71955	1.26231	C	-6.28144	0.2292	0.16936
H	7.0811	-3.2925	0.8053	H	-7.35758	0.25937	-0.29998
C	-6.04971	-1.551	1.93682	C	-3.81653	-2.38979	-2.47405
H	-7.12281	-1.55244	-2.09329	C	-3.25577	-1.51849	-1.50593
H	7.25702	-2.10909	2.09958	N	-1.02456	1.49221	1.63466
C	-0.96415	1.41492	2.97732	N	-1.16092	1.58833	-1.05054
C	-5.24294	-2.38271	-2.66496	N	-3.4888	0.16244	0.18562
H	-5.66935	-3.05125	-3.40475	N	-1.90059	-1.45108	-1.26627
C	-2.92746	-3.21565	-3.20484	N	-1.34292	-1.66134	1.67262
H	-3.31629	-3.89732	-3.95326	N	0.6269	-0.53624	0.32286
C	-1.56493	-3.13788	-2.95494	N	1.69869	-0.0328	-0.27938
H	-0.8625	-3.75455	-3.50194	N	2.76313	-0.74566	0.23594
C	-1.08069	-2.24484	-1.98049	N	5.07622	-1.15777	0.31071
H	-0.0222	-2.1595	-1.77593	S	4.45876	0.80475	-1.39988
C	-5.50087	-0.65733	-0.95132	Ru	-1.38726	-0.06158	0.24318
C	-4.09823	-0.65469	-0.74194				

Table S7. Cartesian coordinates of **Ru-1-O⁻** in the ground state

Ru-1-O⁻							
	X	Y	Z		X	Y	Z
C	32.9486	-57.3637	3.3199	C	31.5385	-53.9901	-1.7093
C	32.735	-58.234	2.3131	C	30.7959	-54.7978	-2.492
C	33.332	-57.9949	0.9827	C	35.7065	-55.4689	-3.5004
N	34.0571	-56.9448	0.783	N	36.1142	-56.0887	-2.4429
C	34.2811	-56.0371	1.8329	C	37.458	-56.5556	-2.3439
C	33.7808	-56.1796	3.0694	C	38.3473	-56.3751	-3.3336
C	35.1163	-54.9094	1.4875	C	37.8997	-55.6734	-4.5435
C	35.4136	-53.9611	2.3884	C	36.6292	-55.2379	-4.6232
C	34.8743	-54.0949	3.7563	C	37.6887	-57.2172	-1.0762
C	34.0974	-55.1515	4.0808	N	36.5833	-57.2793	-0.232
N	35.562	-54.8966	0.154	N	36.8396	-57.8683	0.8237
C	36.2989	-53.9239	-0.2701	N	38.1577	-58.2517	0.7661
C	36.678	-52.8331	0.6518	C	38.7076	-57.8304	-0.4694
C	36.2565	-52.8482	1.932	C	38.8085	-58.9892	1.7647
C	33.1315	-59.9719	-3.5048	S	38.055	-59.5031	3.3449
C	34.3225	-60.1766	-2.9079	C	39.5873	-60.3275	3.8525
C	34.9336	-59.1149	-2.0819	C	40.4828	-60.1619	2.8601
N	34.326	-57.9841	-1.935	N	40.0304	-59.419	1.7167
C	33.0819	-57.772	-2.5536	C	39.8888	-61.0593	5.0768
C	32.4562	-58.6813	-3.3159	C	41.1203	-61.5868	5.205
C	32.4942	-56.4779	-2.2938	C	42.1221	-61.4208	4.1314
C	31.3042	-56.1381	-2.8117	C	41.8292	-60.7398	3.0022
C	30.5968	-57.1199	-3.6577	C	42.8458	-60.5673	1.9004
C	31.1453	-58.331	-3.8978	Ru	34.9549	-56.4457	-0.8896
N	33.2685	-55.6356	-1.4767	O	39.9946	-58.0217	-0.9431
C	32.8404	-54.4521	-1.1851	H	32.5266	-57.5308	4.2674
H	32.143	-59.0876	2.4728	H	33.4054	-53.8103	-0.5788
H	33.1632	-58.6856	0.2123	H	31.1922	-53.0272	-1.4693
H	35.095	-53.3659	4.4809	H	29.8698	-54.4728	-2.8668
H	33.7168	-55.2408	5.0566	H	34.7187	-55.1225	-3.5659
H	36.6326	-53.8967	-1.2636	H	39.3349	-56.7219	-3.2535
H	37.2802	-52.0443	0.3059	H	38.5673	-55.5138	-5.339
H	36.5245	-52.0746	2.5904	H	36.2951	-54.7342	-5.4828
H	32.6936	-60.7244	-4.0927	H	39.1685	-61.171	5.8324
H	34.8207	-61.094	-3.0293	H	41.3734	-62.1214	6.074
H	35.8573	-59.2923	-1.619	H	43.076	-61.8448	4.2595
H	29.663	-56.8768	-4.0748	H	43.7762	-61.0805	2.1466
H	30.6361	-59.0258	-4.5003	H	43.054	-59.5055	1.7605
				H	42.4503	-60.9806	0.9713

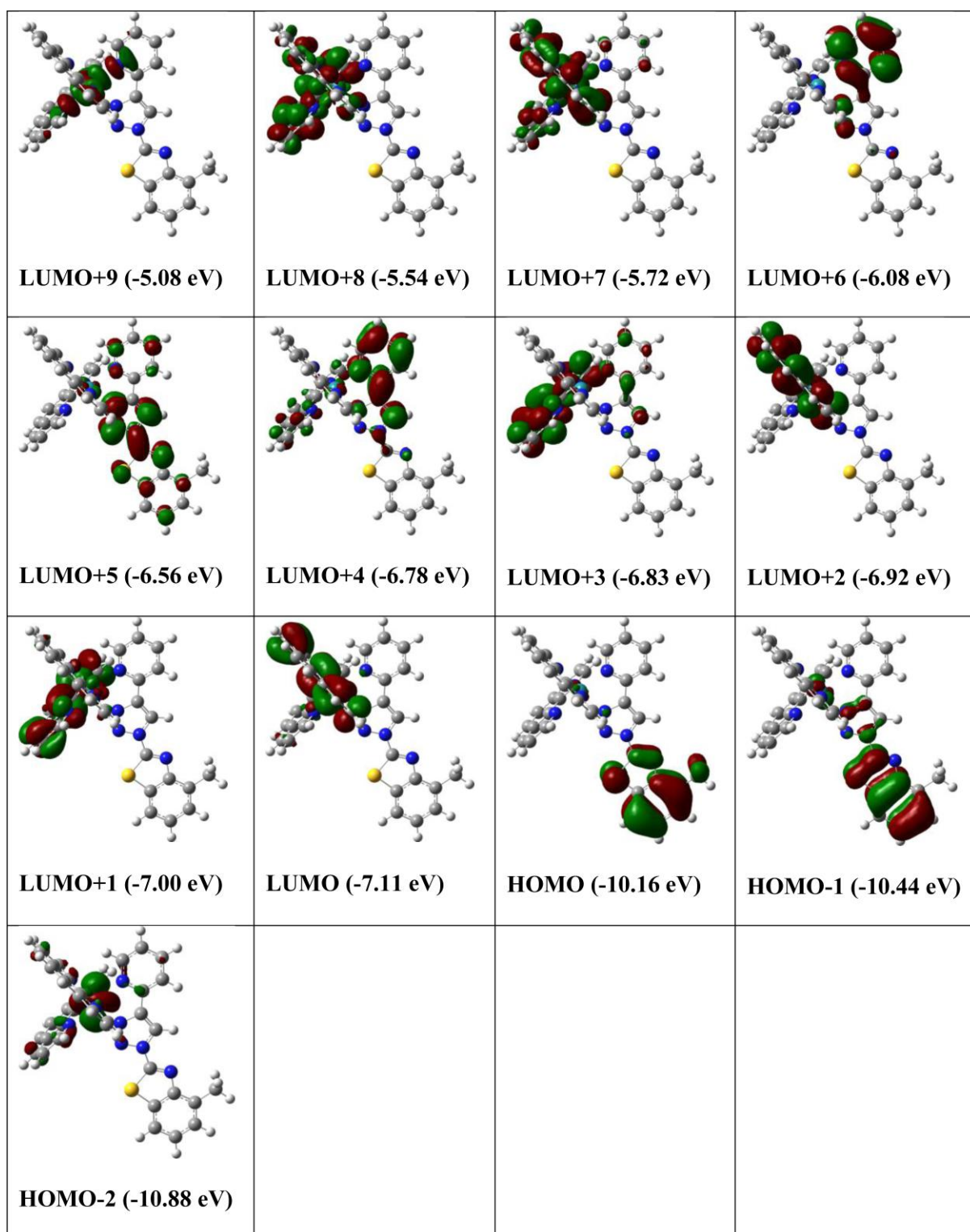


Figure S37. Plots of molecular orbitals HOMO-2 to LUMO+9 for **Ru-1** complex.

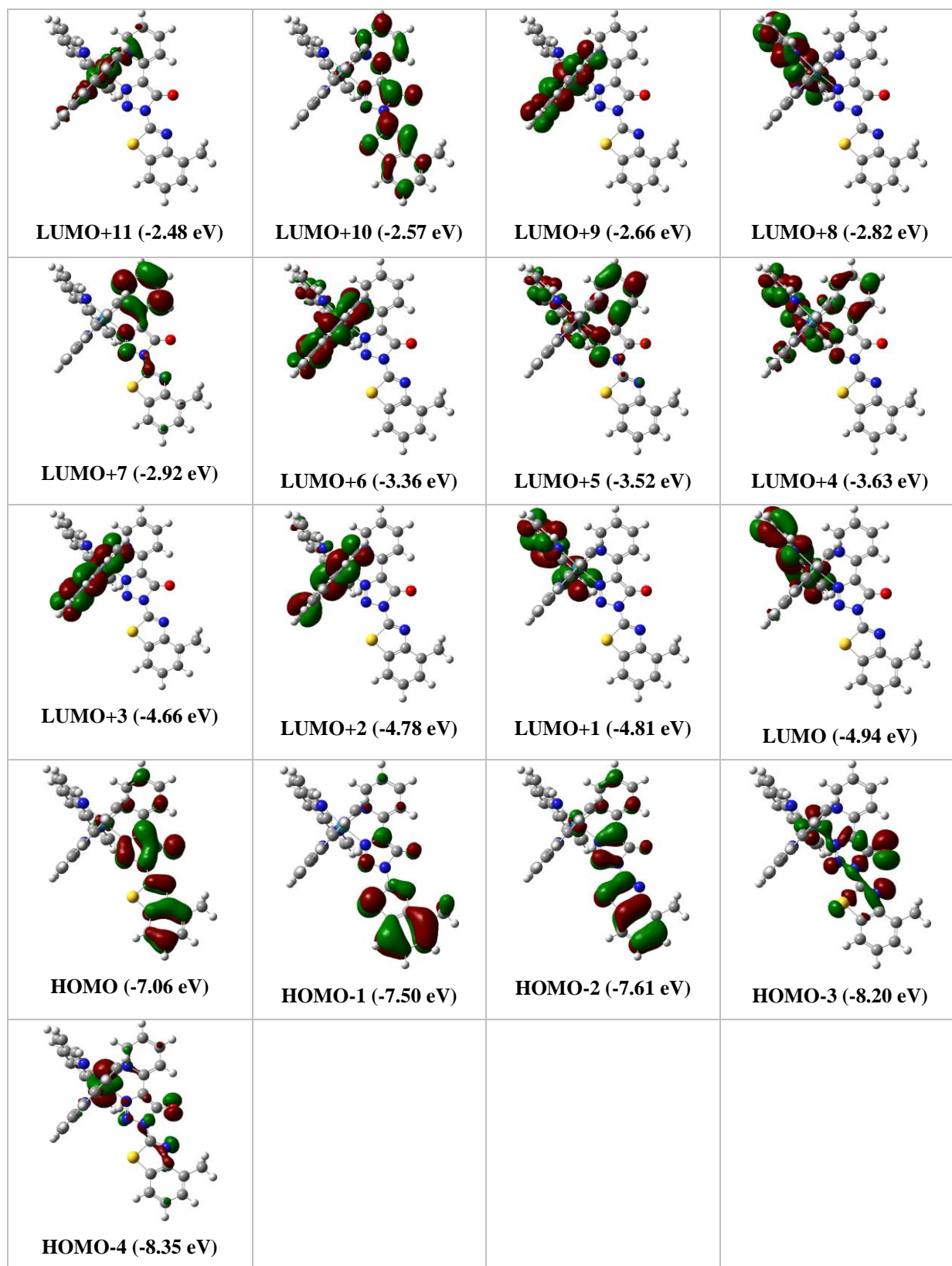


Figure S38. Plots of molecular orbitals HOMO-4 to LUMO+11 for **Ru-1-O[•]** complex.

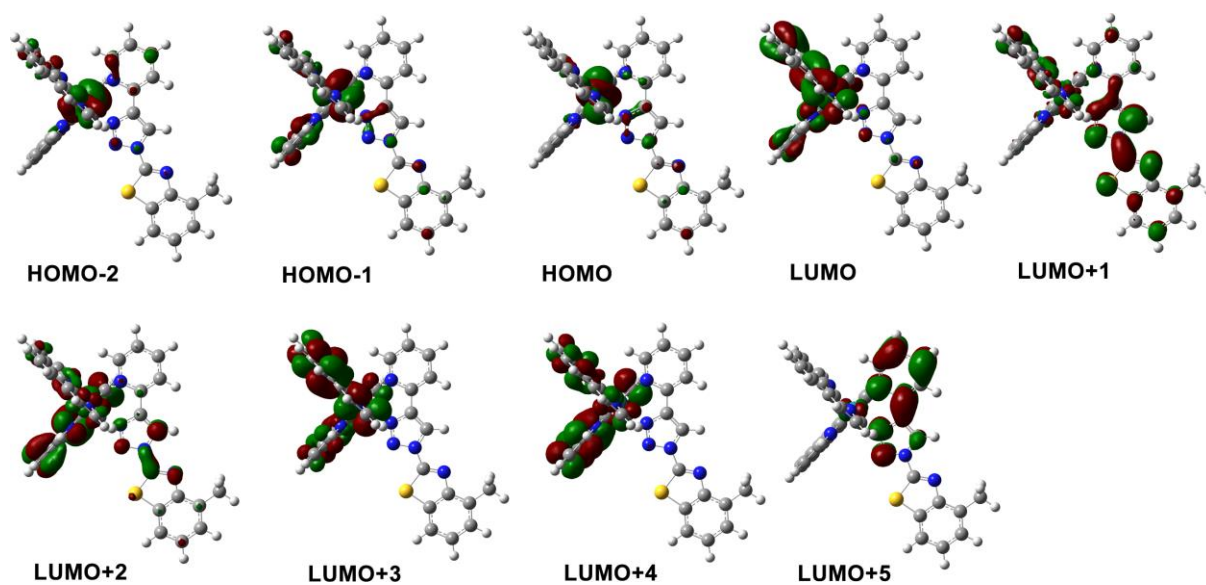


Figure S39. View of the frontier molecular orbitals (MOs) of **Ru-1** obtained from TDDFT calculation [isovalue = 0.03].

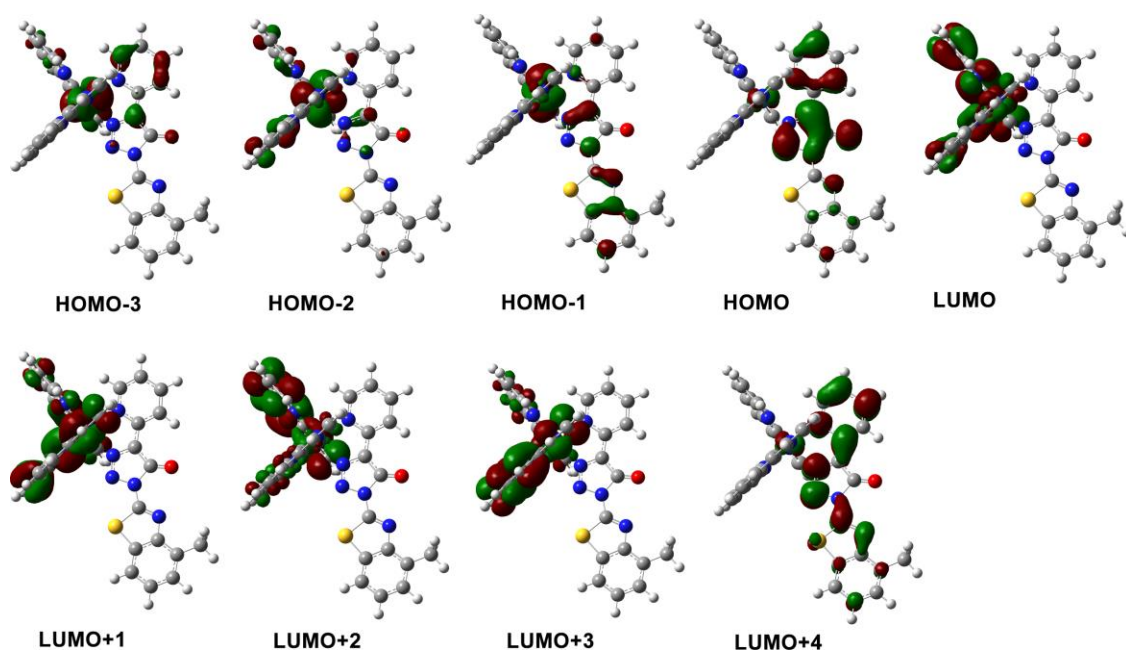


Figure S40. View of the frontier molecular orbitals (MOs) of **Ru-1-O⁻** obtained from TDDFT calculation [isovalue = 0.03].

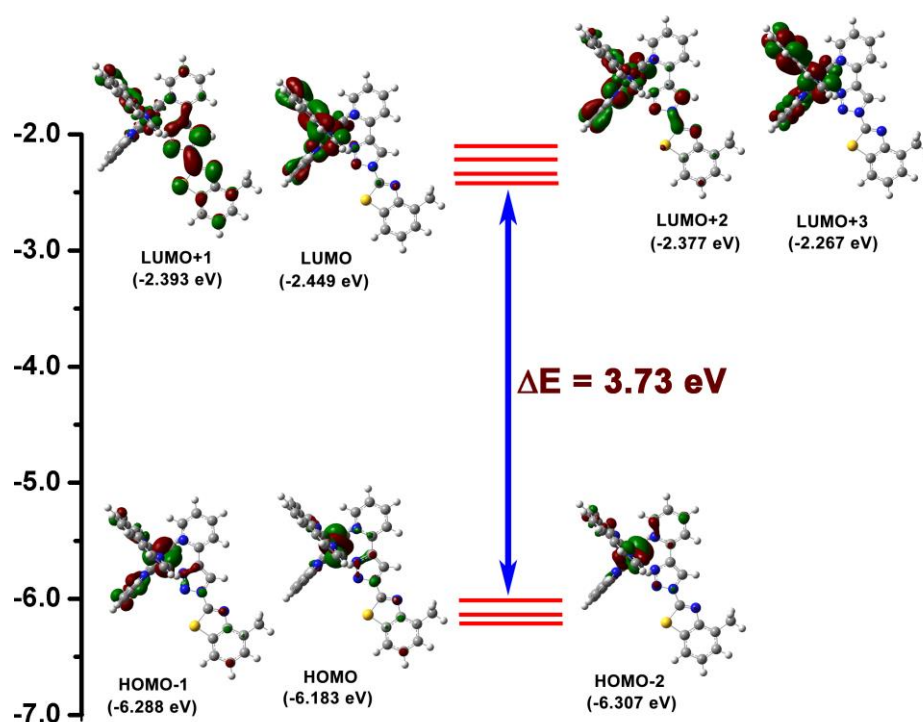


Figure S41. Energy level diagram obtained from TD-DFT (B3LYP/6-31G (d,p) // LANL2DZ) describing the dominant transitions that consisting of the lowest-energy absorption band for **Ru-1** in water.

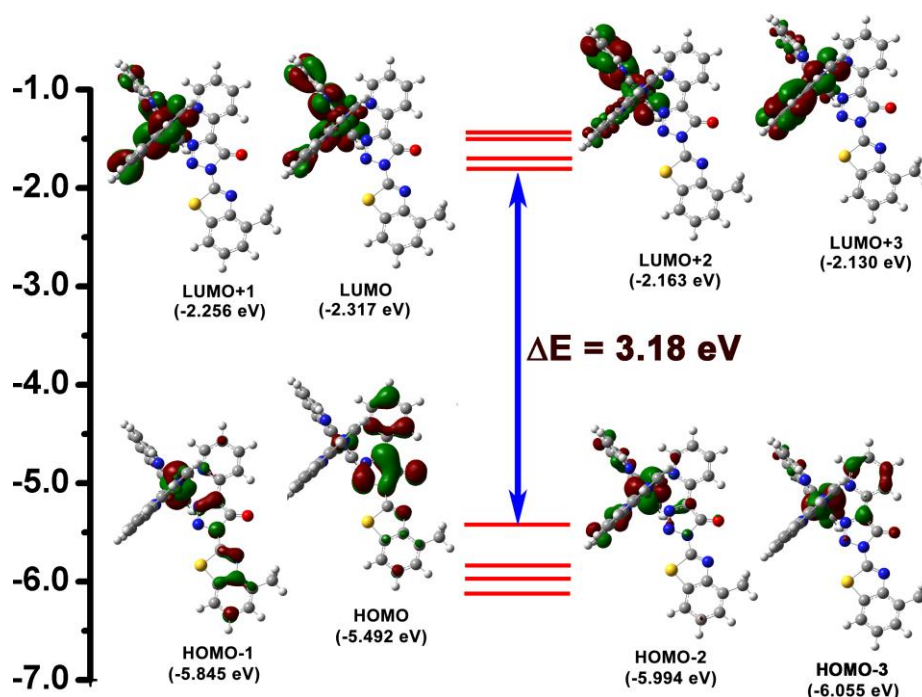


Figure S42. Energy level diagram obtained from TD-DFT (B3LYP/6-31G (d,p) // LANL2DZ) describing the dominant transitions that consisting of the lowest-energy absorption band for **Ru-1-O⁻** in water.

Table S8. Selected transitions obtained from TD-DFT calculation at B3LYP/6-31G (d,p) // LANL2DZ level of **Ru-1** in water.

Complex	State	Energy (eV)	Wavelength ^a (nm)	f^b	Transition	CI ^c	Assignment ^d
Ru-1	S ₁	2.8860	429.61	0.0008	H→L	0.58	MLCT
					H→L+1	0.26	MLCT, ML'CT
					H→L+2	0.27	MLCT, ML'CT
	S ₂	2.9114	425.85	0.0005	H→L+1	0.20	MLCT, ML'CT
					H→L+2	0.55	MLCT, ML'CT
	S ₃	3.0429	407.45	0.0042	H-2→L+2	0.31	MLCT, ML'CT
					H-1→L	0.53	MLCT, ILCT
					H-1→L+1	0.19	MLCT, ML'CT, LLCT
	S ₄	3.0707	403.77	0.0107	H-2→L	0.54	MLCT
					H-1→L	0.12	MLCT, ILCT
	S ₅	3.1019	399.71	0.0327	H-1→L	0.14	MLCT, ILCT
					H→L	0.16	MLCT
					H→L+2	0.11	MLCT, ML'CT
					H→L+4	0.45	MLCT
	S ₆	3.1183	397.60	0.1202	H-2→L	0.29	MLCT
					H-2→L+1	0.23	MLCT, ML'CT
					H-2→L+2	0.31	MLCT, ML'CT
					H→L+2	0.20	MLCT, ML'CT
					H→L+3	0.20	MLCT
	S ₇	3.1587	392.51	0.0320	H-1→L	0.19	MLCT, ILCT
					H-1→L+5	0.11	ML'CT, LL'CT
					H→L+3	0.40	MLCT
					H→L+4	0.11	MLCT
	S ₈	3.1838	389.42	0.0283	H-2→L+2	0.10	MLCT, ML'CT
					H→L+1	0.43	MLCT, ML'CT
					H→L+3	0.27	MLCT
					H→L+4	0.14	MLCT
					H→L+5	0.36	ML'CT
	S ₉	3.2592	380.41	0.0675	H-2→L+5	0.14	ML'CT
					H-1→L+1	0.46	MLCT, ML'CT, LLCT
					H→L+4	0.21	MLCT
	S ₁₀	3.2615	380.15	0.2029	H-2→L+1	0.15	MLCT, ML'CT
					H-1→L+1	0.24	MLCT, ML'CT, LLCT
					H-1→L+2	0.11	MLCT, ML'CT, ILCT
					H→L+3	0.38	MLCT
	S ₁₁	3.2723	378.89	0.0258	H-2→L+1	0.37	MLCT, ML'CT
					H-1→L+2	0.12	MLCT, ML'CT, ILCT
					H→L+4	0.48	MLCT

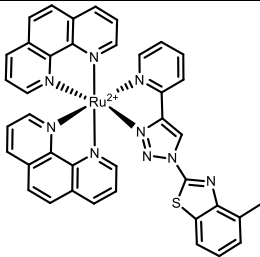
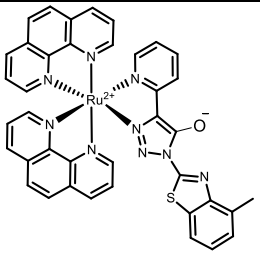
^aOnly the selected low-lying excited states are presented (wavelength >375 nm); f^b = oscillator strength, CI^c coefficients are in absolute values; ^d(MLCT, ML'CT = metal to ligand charge transfer; ILCT = intraligand charge transfer; LLCT = ligand to ligand charge transfer; L = phen, L' = **BtPT**).

Table S9. Selected transitions obtained from TD-DFT calculation at B3LYP/6-31G (d,p) // LANL2DZ level of **Ru-1-O⁻** in water.

Complex	State	Energy (eV)	Wavelength ^a (nm)	<i>f</i> ^b	Transition	CI ^c	Assignment ^d
Ru-1-O⁻	S ₁	2.6267	472.02	0.0040	H→L H→L+1	0.58 0.32	MLCT, L''LCT MLCT, L''LCT
	S ₂	2.6551	466.97	0.0071	H-1→L H→L+1	0.18 0.54	MLCT, L''LCT MLCT, L''LCT
	S ₃	2.7087	457.72	0.0043	H-1→L H→L	0.56 0.23	MLCT, L''LCT MLCT, L''LCT
	S ₄	2.7353	453.28	0.0020	H-1→L H-1→L+1	0.29 0.56	MLCT, L''LCT MLCT, L''LCT
	S ₅	2.8270	438.57	0.0011	H→L+2	0.56	MLCT, L''LCT
	S ₆	2.8606	433.42	0.0020	H→L+2 H→L+3	0.38 0.57	MLCT, L''LCT MLCT, L''LCT
	S ₇	2.8858	429.63	0.0286	H-2→L H-1→L	0.62 0.13	MLCT, ILCT MLCT, L''LCT
	S ₈	2.9623	418.54	0.0164	H-3→L H-3→L+1 H-2→L+1	0.40 0.28 0.38	MLCT, L''LCT MLCT, L''LCT MLCT, ILCT
	S ₉	2.9767	416.52	0.0014	H-2→L+1 H-1→L+2	0.14 0.52	MLCT, ILCT MLCT, L''LCT
	S ₁₀	2.9977	413.59	0.0180	H-3→L+1 H-1→L+2 H-1→L+3	0.47 0.20 0.32	MLCT, L''LCT MLCT, L''LCT MLCT, L''LCT
	S ₁₁	3.0621	404.89	0.1083	H-3→L H-2→L H-1→L+2 H-1→L+3	0.25 0.17 0.20 0.49	MLCT, L''LCT MLCT, ILCT MLCT, L''LCT MLCT, L''LCT
	S ₁₂	3.1188	397.54	0.0257	H-3→L H-2→L+2 H-1→L+2	0.17 0.40 0.25	MLCT, L'LCT MLCT, ILCT MLCT, L'LCT
	S ₁₃	3.2125	385.94	0.1467	H-3→L+3 H-2→L+2 H-2→L+3	0.33 0.43 0.16	MLCT, L''LCT MLCT, ILCT MLCT, ILCT
	S ₁₄	3.2183	385.25	0.0496	H-2→L+3	0.57	MLCT, ILCT
	S ₁₅	3.2372	383.00	0.0474	H-3→L+2 H-2→L+3	0.54 0.31	MLCT, L''LCT MLCT, ILCT
	S ₁₆	3.2757	378.50	0.0827	H-3→L+2 H-3→L+3 H-1→L+4	0.22 0.47 0.21	MLCT, L''LCT MLCT, L''LCT ML''CT, LL''CT

^aSelected low-lying excited states are presented (wavelength >375 nm); ^d(MLCT/ML''CT = metal to ligand charge transfer; IL''CT = intraligand charge transfer; L''LCT = ligand to ligand charge transfer; L = phen, L'' = hydroxylated **BtPT** ligands).

Table S10. Selected Triplet Excited States of probe **Ru-1** and **Ru-1-O[•]** computed by TDDFT at the Optimized Triplet State Geometries.

Complex	Experimentally observed emission energy [eV(nm)]	Computed vertical excitation transition [eV(nm)]	f^a	Transition	Assignment	CI^b
 Ru-1	2.14 eV (580 nm)	2.22 eV (559.56 nm)	0.005	H-5→L	³ MC	0.49
 Ru-1-O[•]	2.11 eV (587 nm)	1.89 eV (654.97 nm)	0.007	H→L+5 H→L+6	³ MLCT/ ³ LLCT ³ MLCT/ ³ LLCT	0.46 0.88

f^a = oscillator strength, CI^b coefficients are in absolute values;

7. Cell viability study and Endogenous HOCl imaging.

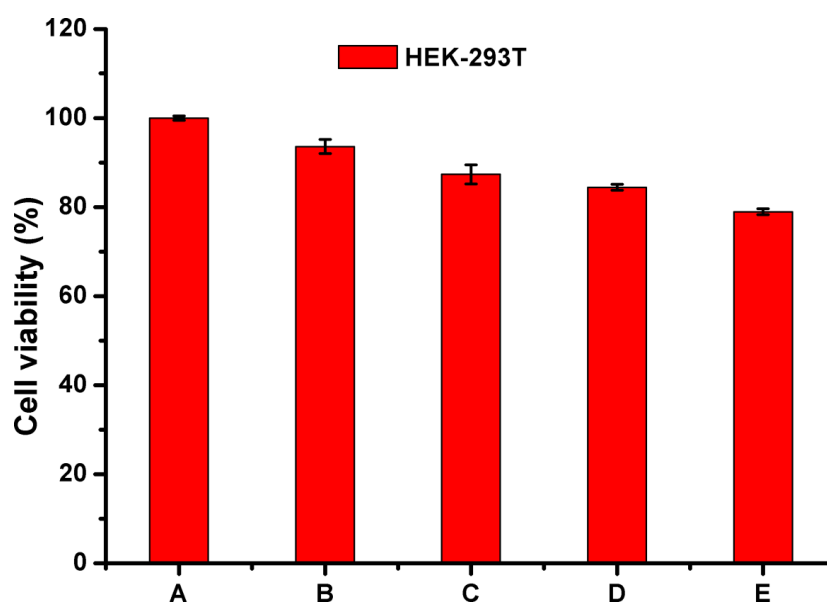


Figure S43. Cell viability was assayed by MTT test with different concentration of **Ru-1** (A: 0 μM; B: 10 μM; C: 25 μM; D: 50 μM; E: 100 μM) in HEK-293T cells. Results are reported as mean ± standard deviation of three independent experiments.

8. References

- [1] Caspar, J. V.; Meyer, T. J. *J. Am. Chem. Soc.* **1983**, *105*, 5583–5590.
- [2] Sheet, S. K.; Sen, B.; Thounaojam, R.; Aguan, K.; Khatua, S. *Inorg. Chem.* **2017**, *56*, 1249–1263.
- [3] Becke, A. D. *J. Chem. Phys.*, **1993**, *98*, 5648–5652.
- [4] Hay, P. J.; Wadt, W. R. *J. Chem. Phys.*, **1985**, *82*, 299–310.
- [5] Cossi, M.; Barone, V. T. *J. Chem. Phys.* **2001**, *115*, 4708–4717.
- [6] (a) Ali, F.; Aute, S.; Sreedharan, S.; H. A. Anila, Saeed, H. K.; Smythe, C. G.; Thomas, J. A.; Das, A. *Chem. Commun.*, **2018**, *54*, 1849–1852; (b) Zhang, X.; Zhao, W.; Li, B.; Li, W.; Zhang, C.; Hou, X.; Jiang, J.; Dong, Y.; *Chem. Sci.*, **2018**, *9*, 8207–8212.
- [7] Chowdhury, B.; Khatua, S.; Dutta, R.; Chakraborty, S.; Ghosh, P. *Inorg. Chem.* **2014**, *53*, 8061–8070.
- [8] Farrugia, L. J. ORTEP-3 for Windows - a version of ORTEP-III with a Graphical User Interface (GUI). *J Appl Cryst.*, **1997**, *30*, 565–568.
- [9] CrysAlisPro Software System, 1.171.36.28; Agilent Technologies UK Ltd.: Oxford, UK, 2013.
- [10] Sheldrick, G. M. *Acta Crystallogr. Sect. A*, **1990**, *46*, 467–473.
- [11] Altomare, A.; Cascarano, G.; Giacovazzo, C.; Guagliardi, A.; Burla, M. C.; Polidori, G.; Camalli, G. *J. Appl. Crystallogr.*, **1994**, *27*, 435–435.
- [12] (a) Sheldrick, G. M. *Acta Crystallogr.* **2008**, *A64*, 112–122; (b) Sheldrick, G. M. SHELXL-97: Program for Crystal Structure Refinement; University of ttingen: ttingen, Germany, **1997**.
- [13] (a) Farrugia, L. J. *J. Appl. Cryst.* **1999**, *32*, 837–838; (b) Farrugia, L. J. *J. Appl. Cryst.* **2012**, *45*, 849–854.